EXPERIMENTAL AND NUMERICAL INVESTIGATION OF SURFACTANT EFFECTS ON THE THERMAL CONDUCTIVITY OF CARBON NANOTUBE NANOFLUIDS

A THESIS SUBMITTED TO
THE GRADUATE SCHOOL OF NATURAL AND APPLIED SCIENCES
OF
MIDDLE EAST TECHNICAL UNIVERSITY

ERDEM DURSUNKAYA

IN PARTIAL FULFILLMENT OF THE REQUIREMENTS
FOR
THE DEGREE OF MASTER OF SCIENCE
IN
MECHANICAL ENGINEERING

JUNE 2016

Approval of the thesis:

EXPERIMENTAL AND NUMERICAL INVESTIGATION OF SURFACTANT EFFECTS ON THE THERMAL CONDUCTIVITY OF CARBON NANOTUBE NANOFLUIDS

submitted by **ERDEM DURSUNKAYA** in partial fulfillment of the requirements for the degree of **Master of Science in Mechanical Engineering Department, Middle East Technical University** by,

Prof. Dr. Gülbin Dural Ünver
Dean, Graduate School of **Natural and Applied Sciences** _____

Prof. Dr. Tuna Balkan
Head of Department, **Mechanical Engineering** _____

Assoc. Prof. Dr. Tuba Okutucu Özyurt
Supervisor, **Mechanical Engineering, METU** _____

Assoc. Prof. Dr. Alpaslan Turgut
Co-supervisor, **Mechanical Engineering, Dokuz Eylül University** _____

Examining Committee Members:

Assoc. Prof. Dr. İlker Tarı
Mechanical Engineering Department, METU _____

Assoc. Prof. Dr. Tuba Okutucu Özyurt
Mechanical Engineering Department, METU _____

Assoc. Prof. Dr. Alpaslan Turgut
Mechanical Engineering Department, Dokuz Eylül University _____

Assoc. Prof. Dr. Almıla Yazıcıoğlu
Mechanical Engineering Department, METU _____

Assoc. Prof. Dr. Barbaros Çetin
Mechanical Engineering Department, Bilkent University _____

Date: _____

I hereby declare that all information in this document has been obtained and presented in accordance with academic rules and ethical conduct. I also declare that, as required by these rules and conduct, I have fully cited and referenced all material and results that are not original to this work.

Name, Last Name: ERDEM DURSUNKAYA

Signature :

ABSTRACT

EXPERIMENTAL AND NUMERICAL INVESTIGATION OF SURFACTANT EFFECTS ON THE THERMAL CONDUCTIVITY OF CARBON NANOTUBE NANOFLUIDS

Dursunkaya, Erdem
M.S., Department of Mechanical Engineering
Supervisor : Assoc. Prof. Dr. Tuba Okutucu Özyurt
Co-Supervisor : Assoc. Prof. Dr. Alpaslan Turgut

June 2016, 83 pages

Nanofluids are suspensions of nanometer sized particles in base fluids. They have been of great interest in heat transfer applications for their unexpectedly superior thermal properties, especially their thermal conductivity. For almost two decades, scientists have been preparing nanofluids with various base fluids and particles, and have been observing their thermal properties and stability. Despite all the research, nanofluids are yet to achieve widespread use because of incoherent research results, stability issues and cost concerns. Carbon nanotubes as nanofluid ingredients seem to offer the highest thermal conductivity enhancement while being also the most challenging ones in terms the maintenance of stability.

This thesis aims to experimentally and numerically investigate the stability and thermal conductivity of carbon nanotube (CNT)-water nanofluids with gum-Arabic as the surfactant. For the experimental part of the study, the transient

hot wire and 3ω methods have been utilized for the thermal conductivity measurements. The stability of the nanofluids have been investigated using sediment photography capturing and scanning electron microscope images. It has been shown that for CNT-in-water nanofluids the use of surfactant is essential for a stable suspension, and that the addition of the surfactant adversely affects the thermal conductivity.

For the numerical investigations, Renovated Maxwell and Hamilton Crosser methods have been adapted for the thermal conductivity estimations. The effect of surfactant layer has been included in the mathematical models. The experimental and numerical results have been compared and a reasonable agreement has been demonstrated.

Keywords: Nanofluid, Carbon nanotube, Surfactant, Thermal conductivity, Transient hot wire, 3ω

ÖZ

KARBON NANOTÜPLÜ NANOAKIŞKANLARDA YÜZEY AKTİF MADDELERİN ISIL İLETKENLİĞE ETKİSİNİN DENEYSEL VE SAYISAL İNCELEMESİ

Dursunkaya, Erdem
Yüksek Lisans, Makina Mühendisliği Bölümü
Tez Yöneticisi : Doç. Dr. Tuba Okutucu Özyurt
Ortak Tez Yöneticisi : Doç. Dr. Alpaslan Turgut

Haziran 2016 , 83 sayfa

Nanoakışkanlar, içerisinde nano boyutlarda parçacık bulunduran sıvılardır. Isıl iletkenlik başta olmak üzere ısıl performanslarındaki üstünlüklerinden dolayı ısı transferi uygulamalarının ilgi odağı olmuşlardır. Biliminsanları yaklaşık yirmi yıldır farklı malzeme ve sıvılarla nanoakışkan hazırlayıp, nanoakışkanların ısıl özelliklerini ve stabilitesini incelemişlerdir. Ancak yapılan sayısız araştırma hala tutarlı sonuçlar vermediği, nanoparçacık üretiminin masrafı ve stabilite sorunlarından dolayı nanoakışkanlar henüz yaygın bir kullanım bulamamışlardır. Karbon nanotüplerin kullanıldığı nanoakışkanlar da en yüksek ısıl iletkenliği sergileseler de, stabilitesinin sağlanması en zor akışkanlardır.

Bu tezde, su içinde karbon nanotüp süspansiyonlarının ısıl iletkenlik ve stabilitelerinin deneysel ve sayısal olarak incelenmesi amaçlanmıştır. Çalışmanın deneysel kısmında ısıl iletkenlik ölçümleri için geçişli sıcak tel ve 3ω yöntemleri

kullanılmıştır. Nanoakışkanların stabilitesi ise, numunelerde oluşan çökeltilerin fotoğraflanması ve taramalı elektron mikroskopi görüntüleriyle incelenmiştir. Su içinde karbon nanotüplü nanoakışkanlarda bir yüzey aktif maddenin kullanılmasının stabilite için çok önemli olduğu, ancak bunun ısıl iletkenlikte bir düşüşe sebep olduğu gösterilmiştir.

Sayısal incelemelerde, ısıl iletkenlik tahminleri için yenilenmiş Maxwell ve Hamilton Crosser modelleri kullanılmıştır. Bu matematiksel modeller kullanılırken yüzey aktif maddenin etkisi de hesaplara katılmıştır. Deneysel ve sayısal sonuçlar karşılaştırılmış ve makul bir tutarlılık sergilenmiştir.

Anahtar Kelimeler: Nanoakışkan, Karbon nanotüp, Yüzey etkin madde, Isıl iletkenlik, Geçişli sıcak tel, 3ω

To my family

ACKNOWLEDGMENTS

I would like to start by thanking my advisor, Dr. Tuba Okutucu for her guidance and support throughout my graduate stuides. I am truly grateful for being her student.

Dr. Alpaslan Turgut has been a very selfless, helping advisor. I would like to thank him for agreeing to be my co-advisor and guiding me in this work at a very critical point.

I have been blessed with being a part of the "Heat Transfer Lab Family". I would like to thank Göker Türkakar for his guidance as a senior, my former roommates Mine Kaya and Ozan Erartsın for making room A-148 a nice place to spend time in, colleagues Onur Özkan, Serhat Bilyaz, Eylül Şimşek, Berke Harmancı, Serdar Hiçdurmaz, Haydar Dirik, Reha Denker, Begüm Elçioğlu, Rahim Jafari and of course, Mustafa Yalçın for being great friends.

I also would like to express my gratitude to Doğacan Koca, Serkan Doğanay and Tuba Evgin, new friends I have made in this 3 year academic journey, for their friendship and help in my work.

Special thanks goes to Emrah Güllü for helping me in writing this thesis using LaTeX.

I would like to thank Dr. Mostafa Kahani, for his hard work during the preparation of the experimental setup.

I had a lot of help from Şahin Coşkun while preparing the nanofluids. I would like to thank him for his help and Dr. Emrah Ünalan and the rest of his students.

This study is financially supported by the Middle East Technical University under grant number ODTÜ-BAP-03-02-2013-002.

Finally, I am very grateful to my father, Dr. Zafer Dursunkaya. I feel privileged for having his guidance as an engineer.

TABLE OF CONTENTS

LIST OF TABLES

TABLES

LIST OF FIGURES

FIGURES

NOMENCLATURE

Symbols

α	m^2/s	Thermal diffusivity
β	-	Volume ratio
C	1/°C	Temperature coefficient of resistance
c_p	kJ/kg·K	Specific heat capacity
γ	-	Mass concentration
d	nm	Diameter
ϵ	-	Eccentricity
h	nm	Layer thickness
I	A	Current
k	W/m·K	Thermal conductivity
κ	-	Empirical Parameter in Renovated Hamilton Crosser model
L	µm	Length
m	g	Mass
n	-	Shape factor
P	W	Power
ϕ	-	Volumetric concentration
ψ	-	Sphericity
q'	W/m	Heat transfer rate per unit length
R	Ω	Resistance
r	nm	Radius, radial
ρ	g/cm^3	Density
T	°C	Temperature
t	s	Time
u	-	Uncertainty

V	V	Voltage
v	nm^2	Parameter associated with thickness in Renovated Hamilton Crosser model

Acronyms

3ω	3-omega
CNT	Carbon nanotube
DWCNT	Double walled carbon nanotube
EG	Ethylene glycol
GA	Gum arabic
HC	Hamilton Crosser
MWCNT	Multi walled carbon nanotube
RHC	Renovated Hamilton Crosser
RM	Renovated Maxwell
SDBS	Sodium dodecylbenzene sulfonate
SDS	Sodium dodecyl sulfate
SWCNT	Single walled carbon nanotube
THW	Transient hot wire

Subscripts

e	Effective
p	Particle
pe	Particle effective
f	Base fluid, fluid
l	Layer
w	Wire

CHAPTER 1

INTRODUCTION

1.1 Motivation

In engineering applications where the transfer of heat is desired, an improvement in the thermal conductivity of the heat transfer medium is desirable. Metals are good conductors of heat whereas gases, due to their low thermal conductivities, are poor conductors. Liquids, in general, have higher thermal conductivities than gases, however, they are primarily used in convective heat transfer applications, which in most cases, require pumping.

The high thermal conductivity of metals was the motivation behind preparing suspensions of small metallic particles in a base fluid to improve the thermal conductivity, in order to enhance the heat transport performance of liquids. This idea dates back to 1873, when Maxwell derived a model for the thermal conductivity of suspensions with metallic particles [1]. Thermal conductivity of such a suspension would depend on the thermal conductivities of both the particles and the fluid, concentration and surface area to volume ratio of the particles.

Although thermal conductivity can be increased by preparing metallic suspensions, this comes with a cost. These suspensions are actually impractical when the particle size is in the order of millimeters or even micrometers because of the potential of clogging. For this reason, suspensions containing larger particles could not be utilized in heat transfer applications.

The idea of metallic suspensions emerged again with the advances in nano-scale manufacturing. It has been possible to produce nanoparticles with very large surface area to volume ratios for approximately 30 years. Choi introduced the idea of suspending nanoparticles in heat transfer fluids like water and oil [2]. This suspension of nanoparticles was soon started to be called *nanofluid*. He argued that nanofluids would not face clogging problems unlike suspensions prepared with millimeter and micrometer sized particles. The research on nanofluids grew rapidly when Choi found the thermal conductivity to be much higher than expected.

Nanofluids can be used in a variety of applications [3]. With the heat dissipation per unit volume increasing rapidly, they can be used in electronics cooling. Because of their higher thermal conductivity, they do not require larger heat transfer areas or faster flow rates to increase the heat transfer rates. With the utilization of nanofluids, up to 40% increase in heat transfer rate has been observed experimentally [4]. The use of nanofluids have been reported in a variety of application including, but not limited to chillers and refrigerators [5], engine cooling, cooling in machining [6] and even medical applications. For instance, ZnO nanofluids are shown to have antibacterial properties [7].

The unusual enhancement in thermal conductivity required an explanation and validation. This requirement resulted in a rapid growth of research on the thermophysical properties of nanofluids. The four most popular explanations are *Brownian motion, nanolayer, thermophoresis* and *clustering of nanoparticles* [8]. *Brownian motion* is the random motion of larger particles –in this case, nanoparticles- caused by collisions with smaller fluid molecules. These collisions result in thermal conduction and its effect on overall conductivity becomes extremely important as particle size decreases [9]. *Nanolayer* is a layer formed around the nanoparticle which acts as a thermal bridge between the particle and the medium. A layer around a substrate embedded in a liquid is reported to be observed by Yu *et al.* [10]. *Thermophoresis* is the diffusion of particles in a medium caused by forces due to a temperature gradient. The final mechanism, *clustering of nanoparticles*, causes a formation of a conduction path in the medium. This mechanism becomes more effective when the particles are slender

as in the case of nanowires and nanotubes.

Although exhibiting extraordinary thermal properties, nanofluids are yet to find a common usage. The first reason is the cost; nanoparticles are still very expensive to manufacture. Another important reason is the increase in pumping power. Nanofluids have higher viscosities than their base fluids as well, which results in requirement of higher pumping power. Often times, heat transfer rate to pumping power ratio is lower for nanofluids than their base fluids [11]. But probably the most important reason is the stability of nanofluids [12, 13]. Due to van der Waals forces, nanoparticles in a nanofluid are attracted to each other, forming aggregates and eventually leading to precipitation [3]. To overcome this problem, either addition of a surfactant or surface treatment of particles is necessary. These measures, however, usually result in lesser thermal conductivity enhancement.

A large variety of nanoparticles have been tested in the preparation of nanofluids, which were initially metals or oxides of metals. Soon after, carbon nanotubes were also started to be used. Carbon nanotubes (CNTs) are tubes solely made of carbon atoms with diameters in the range of nanometers and length in micrometers [14]. They are one of the most popular materials of nanoscience, mainly due to their extraordinary electrical and mechanical properties. They even found commercial use; they are mixed in composites for increased strength and decreased weight, and are also used as coating materials.

CNTs are not only a subject of interest for their mechanical and electrical properties; but also have very high thermal conductivities. Most research report the thermal conductivity of a single nanotube to be over 2000 W/m·K [14, 15]. Some sources report a thermal conductivity of 6000 W/m·K at room temperature [16]. With such a high thermal conductivity, it is prudent to use them as a nanofluid ingredient. Although good conductors, a stable preparation of CNT-water suspension is very difficult due to their hydrophobic surfaces. Further research is required for the case of CNT nanofluids.

The next section presents a portion of research on thermal conductivity of CNT-nanofluids, along with the thermal conductivity models for nanofluids,

and nanofluid thermal conductivity measurement methods, transient hot wire (THW) and 3ω methods.

1.2 Literature survey

The literature survey is presented in three sections. The first section is focused on the experimental thermal conductivity measurements of CNT nanofluids. The second section investigates the methods to measure the thermal conductivity of liquids and the last section presents the models derived to estimate the thermal conductivity of nanofluids.

1.2.1 Thermal conductivity measurements of CNT nanofluids

Nanofluids with CNTs are observed to demonstrate the highest increase in the thermal conductivity [17]. One possible reason for this is the high thermal conductivity of CNT's; researchers report values ranging from 1500 to 10 000 W/m·K [16, 18, 19]. The second argued reason is the high surface area to volume ratio of CNTs. Another popular theory is the previously mentioned agglomeration of particles; since carbon nanotubes are long and slender particles, their agglomeration forms a wireframe of conductance network.

Due to their high surface area and van der Waals forces between them [20], carbon nanotubes rapidly form agglomerates and precipitate when introduced into water. A stable CNT-water solution, however, can be prepared by adding a surfactant or by surface treatment of nanotubes. There are different types of surfactants; most popular ones for CNT-water nanofluids being sodium dodecyl sulfate (SDS), sodium dodecyl benzene sulphonate (SDBS) and gum arabic (GA). Choi *et al.* [21] are the first to prepare a nanofluid with CNT. They have used a synthetic oil as the base fluid, which did not require a surfactant. With a volumetric concentration of 1%, they observed an increase of 150% in thermal conductivity, which is also one of the highest increase for CNT nanofluids in the literature. Transient hot wire method was employed in the measurement.

Instead of using a surfactant, Xie *et al.* [22] chemically treated CNT's in order to prepare nanofluids with base fluids such as ethylene glycol, water and decene. The chemical treatment involved introduction of functional groups that bond to the surface of CNT's, making them repel each other and therefore form a stable solution. Measurements were conducted using the transient hot wire method. For a volumetric concentration of 1%, they reported 19.6%, 12.7% and 7% increase in thermal conductivity for base fluids of decene, EG and water, respectively. They further continued their research with chemically treated CNT's, observing the effect of structure of nanotubes and temperature on the overall thermal conductivity of the nanofluid [23]. In their findings, the highest increase in the thermal conductivity was 27.5%, which was observed at 70°C with ethylene glycol as the base fluid.

Assael *et al.* [24] measured the thermal conductivity of CNT nanofluids in water. They used SDS as the surfactant to investigate the surfactant concentration and sonication. THW method was used for conductivity measurements. The highest increase in thermal conductivity was expectedly observed for the case with the least amount of surfactant. For a 0.6% volumetric concentration of CNT, the result was a 38% increase in the thermal conductivity.

Wen and Ding [25] also investigated the temperature dependence of CNT-water nanofluids. SDBS was used as the surfactant. Measured with THW method, the highest thermal conductivity enhancement was observed to be 31% for a volumetric concentration of 0.84% at 45°C. For 20°C, the increase was about 24%. They also investigated CNT-water nanofluids with GA as the surfactant [26]. The increase in thermal conductivity was about 27% for 1%wt., at 25°C, however, this went up to 80% at 30°C.

Halelfadl *et al.* [27] also investigated CNT-SDBS-water nanofluids. They measured the density, viscosity and thermal conductivity of samples with relatively low volumetric concentrations (ranging from 0.0055% to 0.278%) at 20, 30 and 40°C. The increase in thermal conductivity at the highest concentration was 15% and 38% at 20 and 40°C, respectively.

Hwang *et al.* measured the thermal conductivities of CNT-water nanofluids and

compared their results with those for nanofluids with different particles [28]. Although the thermal conductivity increase was about 11% for a volumetric concentration of 1%, the increase was more than twice that of than nanofluids with SiO_2 and CuO.

Rashmi *et al.* [29] made a comprehensive research on CNT nanofluids with GA. They investigated the effects of temperature, surfactant concentration and sonication on both thermal conductivity and stability of the nanofluid. They reported about 150% increase in the thermal conductivity for 0.1% mass concentration at 25°C, one of the highest increases encountered in the literature.

Sadri *et al.* [30] also investigated the viscosity and thermal conductivity of CNT nanofluids with different surfactants, including GA, with different sonication times. They found a nonlinear increase in the thermal conductivity with an increase in temperature. The highest increase was observed with GA with the longest sonication time (40 minutes); 5% at 25°C and 22% at 45°C.

Another CNT-GA-water nanofluid investigation was carried out by Indhuja *et al.* [31]. In their work, the authors measured viscosity as well and investigated the temperature effects. For a volume concentration of 0.24% and 0.25% of CNT and GA, respectively, there was a 7% increase in thermal conductivity. Thermal conductivity was observed to drastically increase with increasing temperature; a 31% increase at 60°C.

There has been a study on the effect of CNT structure as well. Nasiri *et al.* measured the thermal conductivity of CNT-nanofluids prepared with different type of nanotubes [32]. Results indicated that as the number of walls increase, the thermal conductivity of the prepared nanofluid decrease; in other words, single-walled CNT (SWCNT) nanofluids had the highest conductivity and multi-walled (MWCNT) nanofluids had the lowest. They also investigated the temperature and time dependence of the nanofluids. Results indicated a strong dependence on temperature and time; the conductivity enhancement of SWCNT nanofluids dropped from about 31% to 22% after 400 hours.

A summary of this section is tabulated in Table 1.1.

Table 1.1: Summary of CNT-nanofluid experiments in the literature

Researchers	Year	Base fluid	Conc.	Surfactant	Enhancement, $(k_e - k_f)/k_f$
Choi *et al.* [21]	2001	poly-olefin	1% vol.	-	150%
Xie *et al.* [22]	2003	water	-	Surface Treatment	7%
		EG			12.7%
		Decene			19.6%
Xie *et al.* [23]	2009	EG	-	Surface Treatment	22 % at 20°C
					27.5% at 70°C
Assael *et al.* [24]	2004	water	0.6% vol	SDS, 0.1% wt.	38%
				2% wt.	30%
Wen and Ding [25]	2004	water	0.37% vol.	SDBS	15% at 20°C
			0.84		21%
			0.37		23% at 45°C
			0.84		31%
Ding *et al.* [26]	2006	water	1% wt.	GA	27% at 25°C
					80% at 30°C
Halelfadl *et al.* [27]	2013	water	0.0056% vol.	-	4% at 20°C
					14% at 40°C
			0.278%		15 at 20°C
					38% at 40°C
Hwang *et al.* [28]	2006	water	1% vol.	SDS	11.3%

Table 1.1: Summary of CNT-nanofluid experiments in the literature (continued)

Rashmi *et al.* [29]	2011	water	0.01% wt.	GA	105% at 25°C 160% at 60°C
			0.1		150% at 25°C 240% at 60°C
Sadri *et al.* [30]	2014	water	0.5% wt.	GA	5% at 20°C 22% at 45°C
Indhuja *et al.* [31]	2013	water	0.14% vol.	GA	2% at 28°C 26% at 60°C
			0.24%		7% at 28°C 31% at 60°C
Nasiri *et al.* [32]	2012	water	0.24%	Surface Treatment	8% for MWCNT 21% for SWCNT

1.2.2 Transient hot wire method

A detailed investigation of THW method will be presented later in the thesis. In this section, some highlights from the literature will be presented.

THW method is the predominantly used thermal conductivity measurement method for liquids, however, cases where it is used for gases are also present [33]. For nanofluids, about 65% of the measurements are taken using the transient hot wire method [34].

Basically, THW method uses a line source (usually a platinum wire), which acts as line heat source and a thermometer. The sample is heated for a period of time, which also results in a temperature increase in the wire. The thermal

conductivity of the fluid can then be found from this temperature change. There are two main advantages of this method; the first one is the time needed for measurement is short. The other is the minimization of any convection effects.

Using the THW method requires some assumptions. The first assumption is that the hot wire is an infinitely long, negligibly thin line source with uniform heat dissipation. The validity of these assumptions were investigated by Kierkus *et al.* [36]. They have listed the conditions for which the THW method gives acceptable results.

One problem with this method occurs when the sample liquid is electrically conductive. Since there is an electrical current flowing through the wire, if the liquid is electrically conductive, then the current might flow through the liquid, which can result in great errors. Nagasaka and Nagashima [37] coated the wire with a thin insulation layer and showed that the effect of this layer on the results is negligible if the rest of the system is built carefully. A hot wire with a thin insulation is extensively used for nanofluids [24, 28, 38, 39].

Another thing to be wary of is the thermal expansion of the wire. Since the change in electrical resistance is measured to deduce the temperature change of the wire, stress induction due to heating will cause an extra change in the resistance (strain gage effect). Researchers have developed methods to minimize this effect. For example, Assael *et al.* used the same material for both the wire and the wire holder [24], while Kostic and Simham used a tension spring [38].

1.2.3 3ω method

3ω is a thermal conductivity measurement method not limited to liquids. It was originally developed for thermal diffusivity measurements of metal filaments similar to those used in incandescent light bulbs [40]. Currently it is being widely used for measuring the thermal conductivity of thin films and solid substrates [41].

Only a few of the studies in the literature use 3ω to measure the thermal conductivity of nanofluids. Oh *et al.* [41] microfabricated a 3ω device to measure

the thermal conductivity of Al_2O_3 nanofluids. Only a droplet of the sample is enough for an accurate measurement for their device. The maximum increase observed was for the DI water with 0.4% volumetric concentration of Al_2O_3, where there was an 11.3% increase in the thermal conductivity.

Turgut *et al.* [42] measured the thermal conductivity of water-TiO_2 nanofluids with the 3ω setup they have built. Authors report a 2.5% increase in thermal conductivity for 1% volumetric concentration.

Only two studies has been encountered on measurement the measurement of thermal conductivity of CNT nanofluids using 3ω method. First one is the work of Wu *et al.* where humic acid was the base fluid [43]. Second one is the work of Choi *et al.* [44], where they report an increase in thermal conductivity by 19.4% for a volumetic concentration of 1.14%. The most recent work found on the use of 3ω method was conducted by Chirtoc *et al.* [45], although the measured samples are vegetable oils instead of nanofluids. Measurements were carried out in elevated temperatures.

3ω method deals with very small temperature differences, which results in elimination of convection effects in measurements. It is also possible to make good measurements with very small amount of samples [46]. However, this method requires sophisticated electronic components for voltage measurement, therefore it is very expensive. For this reason, 3ω is not a widely used thermal conductivity measurement method for liquids.

1.2.4 Thermal conductivity models for nanofluids

Like in any other branch of science, experiments are usually expensive and time demanding. This is also valid for science of nanofluids; nanomaterial production is still far from cheap, considering the number and amount of samples needed to observe the effects of several parameters. Therefore a thermal conductivity model for nanofluids would be a very useful tool in thermal engineering.

One of the earliest model is Maxwell's effective thermal conductivity model for spheres in a medium [1]. Based on effective medium theory, this model did

not take the size and shape of particles into account and was proven to fail for volumetric concentration ratios above 25%, however, this model formed the basis of many models for thermal conductivity of composite materials. One of these models is Hamilton-Crosser's model [47]. The difference of this model from Maxwell's is that the effect of particle geometry is considered. Instead of spheres, particles are treated as ellipsoids.

These models were derived for macro sized particles and they were found to underestimate the thermal conductivity of suspesions of nano sized particles. Therefore researchers began to develop new models.

Yu and Choi [48, 49] developed two of the earliest nanofluid thermal conductivity models. These models were based on previously mentioned Maxwell and Hamilton-Crosser models, with an addition of the nanolayer effect. They argued that a nanolayer made up of the base fluid molecules is formed around the particle. These molecules are more ordered than in liquid form, therefore the layer has a higher thermal conductivity than the base fluid, resulting in nanolayer acting as a thermal bridge and therefore increasing the overall thermal conductivity of the fluid. Although these two models account for nanolayer, they had a downside; the thickness and the thermal conductivity of the nanolayer had to be determined experimentally. The renovated Hamilton-Crosser additionally required the shape factor of the particles as well.

Wang *et al.* [50] considered the effect of clustering and derived a model based on effective medium theory and fractal theory. In the model, the particles are assumed to form clusters and the thermal conductivity of these clusters are calculated. This model took the effects of particle size and particle surface adsorption into account.

Nan *et al.* [51] also derived a simple model based on effective medium theory. With their model, they argued that unlike the common belief in the literature, the effective medium theory succeeds in explaining the abnormal increase of thermal conductivity. Later revision of the model included Kapitza resistance effects and revealed that this drastically reduces the increase in thermal conductivity [52].

Thermal conductivity models based on effective medium theory are but a fraction of thermal conductivity models derived for nanofluids. For example, Jang and Choi derived a model taking nano-scale heat transfer and Kapitza resistance into account, emphasizing the role of Brownian motion [9]. Bhattacharya *et al.* [53] also worked on Brownian motion effect, using Brownian Dynamics Simulation to derive a thermal conductivity model.

Instead of using effective medium theory, Murshed *et al.* [54] solved the heat transfer equation in spherical coordinates for nanofluids with nanolayer. However, the problem of unknown layer thickness and thermal conductivity still persists in their model. They continued their research by further developing their model to include particle interaction and Brownian motion effects [55]. Xie *et al.* [56] also derived a model including the effect of a nanolayer around spherical nanoparticles. They assumed the thermal conductivity of nanolayer is a linear function of particle radius, with being equal to that of particle and liquid at the inner and outer surfaces of the layer, respectively.

Tillman and Hill [57, 58] proposed a new method with the purpose of filling the void in nanolayer based models; the thickness and thermal conductivity of the nanolayers. They proposed that the nanolayer thermal conductivity is a function of nanolayer thickness. For spherical layered particles, they have solved the heat conduction equation and determine the thickness from the solution of the resulting differential equation.

Patel *et al.* derived a model for the thermal conductivity of CNT nanofluids [59]. Novelty in their model was the inclusion of CNT agglomeration effects. This model however, overpredicted the thermal conductivity, probably because of the spherical particle and isotropic thermal conductivity assumption. A recent study by Thang *et al.* modified their model to take CNTs as cylindrical particles with anisotropic thermal conductivity [60]. A model that includes both nanolayer and agglomeration effects is also present in the literature [61].

Models that include the surfactant effects are quite rare. An example is the work of Yang and Du [62]. Their model is largely based on the model derived by Murshed *et al.* [54]; this model replaced the nanolayer with a surfactant layer.

This section covered numerous models, but not all in the literature. As can be seen, there is a great amount of effort spent on modeling of nanofluid thermal conductivity. However, due to the inconsistency of numerous experimental values, none of these models can be of general use for the estimation of thermal conductivity of nanofluids. Almost all of the models choose different experimental data to compare their models with.

1.3 Scope of thesis

Surfactants are indispensable when preparing stable CNT-water nanofluids. Therefore it is a necessity to consider their effects on thermal conductivity. This work aims to respond to this need by modifying readily available models to include surfactant effects. These modified models replace the liquid nanolayer with a surfactant layer. A parametric study using these modified models to investigate the surfactant effects is conducted.

This work also aims to investigate the effect of surfactant on the thermal conductivity of CNT-water nanofluids experimentally. A setup based on THW method, the most commonly used liquid thermal conductivity measurement method, was built for measurements and investigated in detail. A 3ω setup was also used to repeat the measurements. The measurement results have been compared to available ones in the literature. Experimental results have also been compared to the results from the modified models.

1.4 Outline

This thesis is divided into 5 chapters. Chapter 2 comprises the experimental aspect of the thesis; detailed explanation of the experimental setup, transient hot wire and 3ω theories, and nanofluid preparation. Chapter 3 is the explanation of theoretical conductivity models used in this work for comparison; Renovated Maxwell and Hamilton Crosser models. Presentation of the results, literature comparison and discussion is presented in Chapter 4 and further comments on

the subject and future work are explained in Chapter 5.

CHAPTER 2

EXPERIMENTAL WORK

2.1 Transient hot wire method

2.1.1 Theoretical background

Transient hot wire method involves a wire embedded in a medium, which is the liquid the conductivity of which will be measured. The wire is assumed to be infinitely long and thin line source, with high conductivity and low heat capacity and the liquid is infinite and incompressible, therefore heat transfer occurs solely in the radial direction and there is only conduction heat transfer in the system.

With these assumptions, the heat conduction equation in cylindrical coordinates is written as follows;

$$\frac{1}{\alpha_f}\frac{\partial T}{\partial t} = \frac{1}{r}\frac{\partial}{\partial r}\left(r\frac{\partial T}{\partial r}\right) \tag{2.1}$$

With the following boundary conditions;

$$T(r, t = 0) = 0 \tag{2.2a}$$

$$\lim_{r\to 0}\left\{r\frac{\partial T}{\partial r}\right\} = -\frac{q'}{2\pi k_f} \tag{2.2b}$$

$$\lim_{r\to\infty} T(r, t) = 0 \tag{2.2c}$$

where T is the temperature, α_f and k_f are the thermal diffusivity and thermal

conductivity of the fluid to be measured, respectively, and q' is heat dissipation rate per unit length.

Carslaw and Jaeger [35] give the solution of this problem;

$$T(r,t) = \frac{q'}{4\pi k_f} \int_{r^2/(4\alpha_f t)}^{\infty} \frac{e^{-u}}{u} du \tag{2.3}$$

Provided that $r^2/(4\alpha_f t) << 1$, Equation 2.3 can be approximated as follows;

$$T(r,t) = \frac{q'}{4\pi k_f} \left[\ln\left(\frac{4\alpha_f t}{r^2}\right) - g \right] \tag{2.4}$$

where g is Euler's constant and is equal to 0.5772... .

After a short initial transient period, thermal conductivity of the fluid can be found from the slope of Equation 2.4 for a time range between t_1 and t_2 as;

$$k_f = \frac{q'}{4\pi(T_2 - T_1)} \ln\left(\frac{t_2}{t_1}\right) \tag{2.5}$$

where t_1 represents the end of initial short transient period. In practice, heating the medium long enough will result in emergence of convection effects; therefore t_2 is the time when convection effects occur, and the linear proportionality between T and $\ln(t)$ is disrupted.

The linear relationship between T and $\ln(t)$ is shown in Figure 2.1.

In practice, THW employs a wire that acts both as a line source and a temperature sensor. In order to act as an ideal line source, the wire should be thin, have high conductivity and relatively low heat capacity.

The change in the temperature of the wire is measured from the change in its electrical resistance. For platinum, this relation is known over a wide temperature range. This is the reason why platinum is the most widely used material for hot wire.

While using THW method, there should be an insulation layer around the wire if

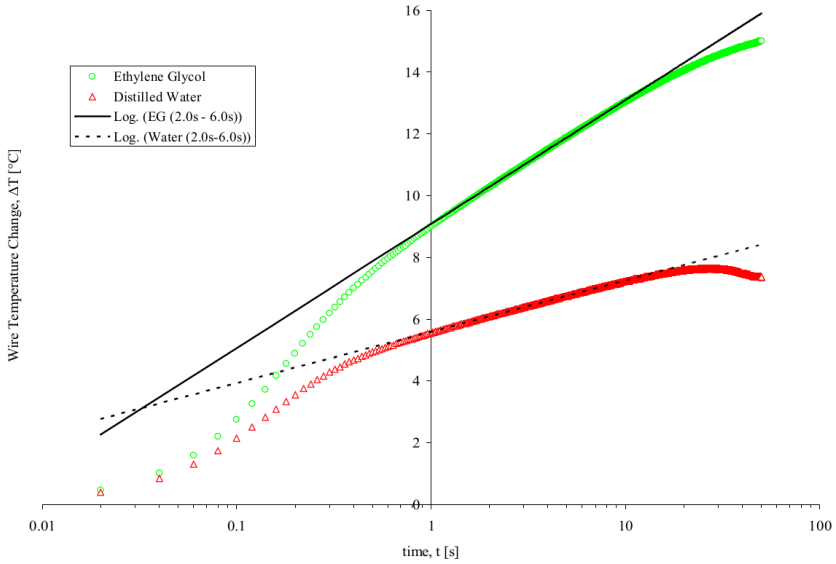

Figure 2.1: Relation between T and $\ln(t)$ in THW [38]

the fluid is electrically conductive. Otherwise, current can flow through the fluid, changing the heat transfer problem of the system. To overcome this problem, Nagasaka and Nagashima [37] designed a hot wire system with an insulation layer and analyzed its effects both theoretically and experimentally. They found out that the effect of insulation layer is negligibly small if the system was adequately designed. By solving the conduction equation problem in a layered cylinder, they found the temperature rise in the wire as

$$\Delta T = \frac{q'}{4\pi k_f}\left[\ln(t) + A + \frac{1}{t}\left(B\ln(t) + C\right)\right] \tag{2.6}$$

where A, B and C are constants. When t value is large enough, the $(B\ln(t)+C)$ term can be neglected and the slope of the resulting equation can be used to find k_f, as in Equation 2.5.

Yu and Choi [63] also investigated the effect of coating both theoretically and experimentally. They found out that the measurement error due to coating is negligibly small even for insulation thicknesses comparable to wire diameter.

2.1.2 Experimental setup

The constructed experimental setup is given in Figure 2.2. A DC power supply (Figure 2.3b) provides power to the circuit. There is a Wheatstone bridge in the circuit with two resistors with known resistances, a resistor with controllable resistance (a potentiometer), and a resistor of unknown resistance, which in this case is the platinum wire inside the sample. Data acquisition system is used to measure the voltage difference across the bridge to measure the change in resistance of platinum wire, and eventually its temperature.

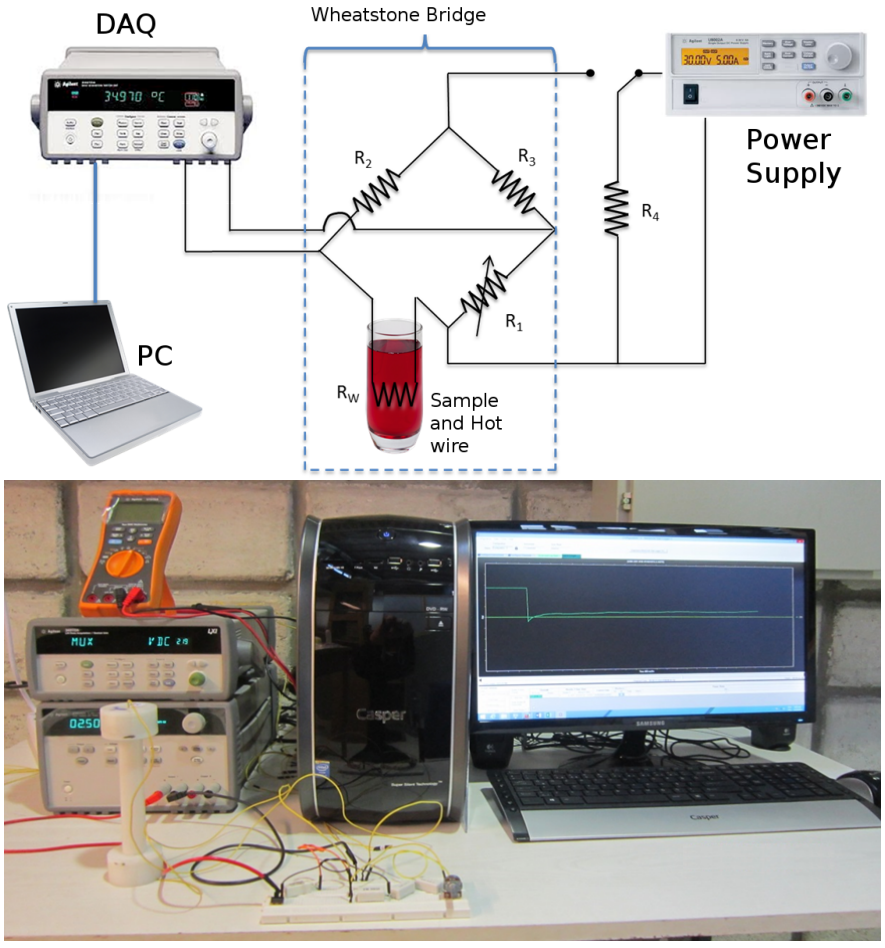

Figure 2.2: THW setup

The bridge is initially balanced; in other words, the potentiometer is adjusted such that there is no voltage difference across the bridge, which is achieved when

$$\frac{R_w}{R_2} = \frac{R_3}{R_1}. \tag{2.7}$$

With voltage reading across the bridge, R_w can be found as

$$R_w = \frac{(V_p + V_b)R_1 + V_b R_3}{-V_b R_1 + (V_p - V_b)R_3} R_2 \tag{2.8}$$

where V_p is the voltage supplied to the circuit by power supply and V_b is voltage reading across the bridge.

A photograph of the circuit, excluding the hot wire cell, is shown in Figure 2.4. Ceramic resistors were used instead of regular ones because of their durability under high currents.

Figure 2.5 is the hot wire cell. It was manufactured in the machine shop of Mechanical Engineering Department. The material used is for the cell is teflon. Holder (Figure 2.5b) was designed to electrically connect the platinum wire with the circuit and to keep the wire straight inside the cell. The setup was also designed to measure the thermal conductivity of the sample at different temperatures by embedding the hot wire cell into a temperature controlled bath. Therefore the holder was also designed to prevent any leakage inside the cell, by adding a cut on the circumference for the O-ring. Platinum wire is held between the aluminum parts, which are tightened by the screws on the side of the holder. The electrical connection is established through these screws and cubes. The technical drawings of the hot wire cell are provided in Appendix A.

The wire used as the hot wire was purchased from A-M systems. A photograph of the wire is shown in Figure 2.6. Two types of wires were tested for the setup. These wires were readily insulated. The insulation materials are Isonel and PFA, which are types of polyester and teflon, respectively. Properties of the wires are tabulated in Table 2.1.

(a) Agilent 34972A DAQ System

(b) Agilent E3648A Power Supply

Figure 2.3: DAQ System and power supply used in setup

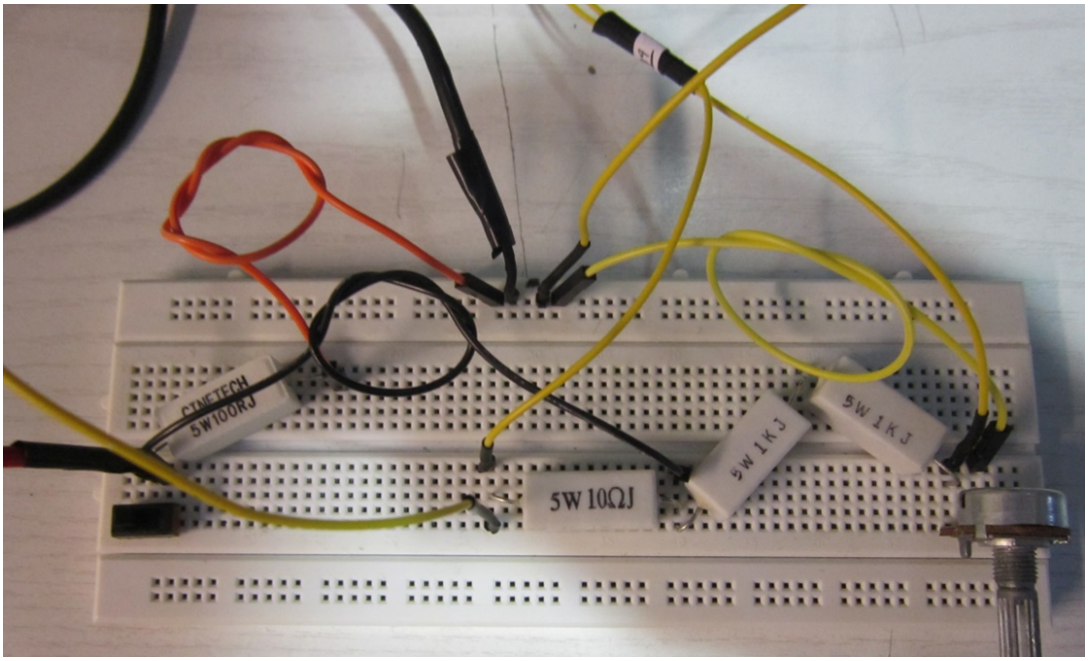

Figure 2.4: Circuit of the THW setup

Table 2.1: THW method wire properties

Data	Wire 1	Wire 2
Bare diameter (µm)	25.4	76.2
Coated diameter (µm)	27.94	139.7
Coating material	Isonel	PFA
Thermal conductivity, W/m·K	71.6	
Temp. coeff. of resistance, $°C^{-1}$	3.93×10^{-3}	

2.1.3 Experimental procedure

The measurement procedure starts with the placement of the wire. Approximately 20 cm of wire is cut and 12 cm of it is embedded in the sample inside the cell. Then the coating at one end of the wire is removed by applying heat. The wire is then passed through the middle hole on the holder (Figure A.1) with the uncoated portion being in the rectangular cut of the holder. The hole is then sealed with small amount of silicon to prevent the sample from contacting the uncoated portion. After sealing the hole, wire is tightened between the aluminum cubes for electrical contact. The free end of the wire is then passed

(a) Whole view

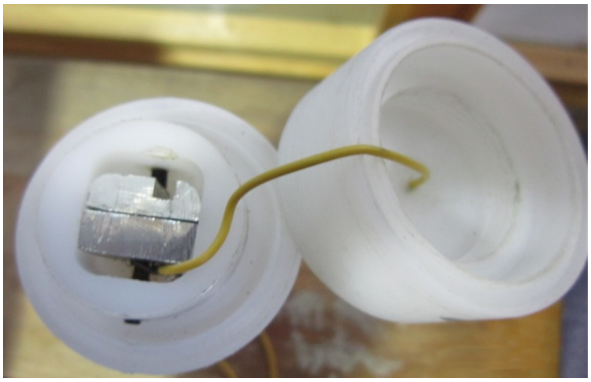

(b) Holder

Figure 2.5: Hot wire cell of the THW setup

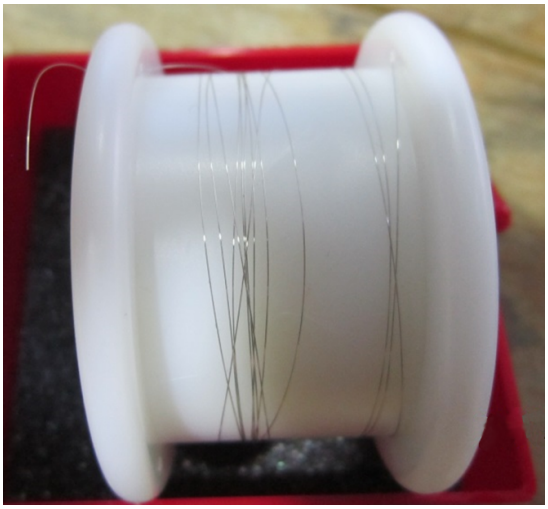

Figure 2.6: Platinum wire

through the cylindrical cell, and again from the center hole of the second holder. The coating on this tip is again removed and the wire is tightened between the aluminum cubes. This time, however, some tension on the wire is applied in order to keep the wire straight inside the cell. When the placing of the wire is complete, sample is injected through the eccentric hole on the upper holder. One of the aluminum cubes has a cut for accessibility to this hole (Figure 2.5b).

The cell is connected to the circuit through copper wires. These wires are connected to the aluminum cubes through the screws that are pressing aluminum cubes to each other.

After the completion of the circuit, the Wheatstone bridge has to be balanced. This is done by applying minimal voltage on the circuit and adjusting the potentiometer such that the voltage reading across the Wheatstone bridge is close to zero (on the order of microvolts).

When the balancing of the bridge is complete, the power supply is turned on. The switch initially completes the dummy circuit, that consists of solely R_4, until the DAQ is ready for the measurements. When the data acquisition process is started from the computer, the switch is switched to complete the Wheatstone bridge circuit.

2.2 3ω method

2.2.1 Theoretical background

3ω method is another transient method for the measurement of thermal conductivity. For liquids, 3ω method is actually very similar to THW method, since both methods involve a line source that also acts as a temperature sensor. The difference is that the wire is excited with an alternating current in 3ω method instead of a direct current;

$$I(t) = I_0 \cos(\omega t) \tag{2.9}$$

where ω is the frequency of the current. In practice, R changes with the wire temperature, therefore the resistance oscillation is given as

$$R(t) = R_0(1 + C\Delta T_{\mathrm{DC}} + C|\Delta T_{\mathrm{AC}}| \cos(2\omega t + \theta)) \tag{2.10}$$

where C is the temperature coefficient of resistance. Thus the time dependent voltage across the resistance becomes,

$$V(t) = I_0 R_0[\cos(\omega t) + 0.5C|\Delta T_{\mathrm{AC}}| \cos(\omega t + \theta) + 0.5C|\Delta T_{\mathrm{AC}}| \cos(3\omega t + \theta)] \tag{2.11}$$

Equation 2.11 shows that the voltage variation has a third harmonic of frequency of 3ω. Therefore, it is possible to deduce the temperature response from the voltage by measuring the voltage across the wire. The amplitude of 3ω component is small, but can be measured with proper equipment.

The temperature oscillation profile of the medium with heat generation from a line source that is excited by an alternating current is given by Carslaw-Jaeger [35]:

$$\Delta T = \frac{P}{L_w \pi k} K_0 \left(\sqrt{\frac{i2\omega}{\alpha}} r \right) \tag{2.12}$$

where P is the power dissipation in the wire, L_w is the wire length and K_0 is the modified Bessel function of the order zero. When the argument of K_0 in Equation 2.12 is much less than 1, Equation 2.12 can be approximated by [64]

$$\Delta T = -\frac{P}{L_w \pi k} \left[\ln \left(1.26 \sqrt{\frac{\omega}{\alpha}} r \right) + i \frac{\pi}{4} \right] \tag{2.13}$$

Similar to the assumptions in transient hot wire method, 3ω method also assumes infinitely long and thin line source so that heat transfer occurs only in radial direction. The medium is also assumed to be infinite.

Additionally, the wire to be used has to have high thermal conductivity and low heat capacity for guaranteeing of all the heat generated is dissipated into the medium. A high frequency current will also result in storage of heat in the vicinity of the wire, and therefore should be avoided. High amplitudes of ΔT oscillations should also be avoided to prevent any convective heat transfer due to high temperature gradients.

2.2.2 Experimental setup

3ω measurements were carried out in Assoc. Prof. Dr. Alpaslan Turgut's laboratory in Mechanical Engineering Department of Dokuz Eylül University.

Schematic of the setup is given in Figure 2.7.

The lock-in amplifier acts as a wave generator for the circuit and also enables voltage measurement across the Wheatstone bridge. It measures both the amplitude and the phase angle of the 3ω component of voltage across the wire. The phase angle can be used to determine the thermal diffusivity of the fluid [46]. The amplitude of this 3ω component is on the order of few hundred microvolts. The lock-in amplifier used in this work is a Stanford SR850 lock-in amplifier (Figure 2.8).

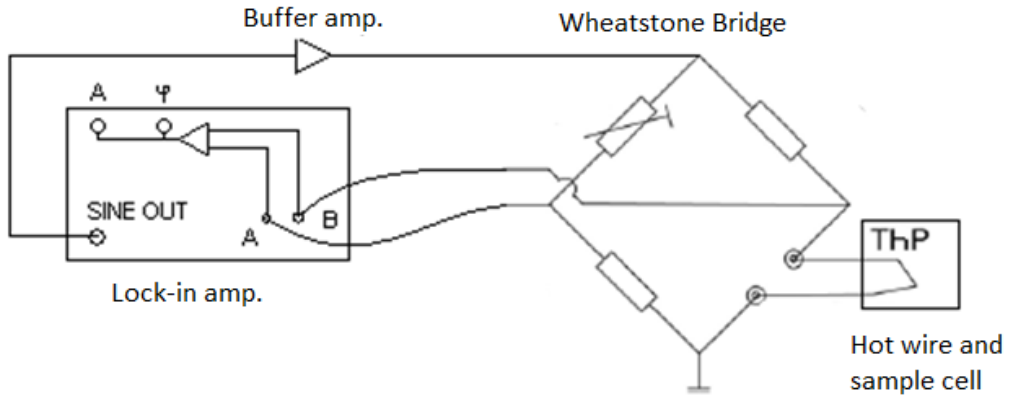

Figure 2.7: Schematic of 3ω measurement setup

Figure 2.8: Stanford SR850 digital lock-in amplifier

Circuit including the Wheatstone bridge can be seen in Figure 2.9. There is a buffer amplifier to amplify the signal generated by the lock-in amplifier and this power is drawn from an external power supply.

The hot wire immersed in the sample can be seen in Figure 2.10. The wire used

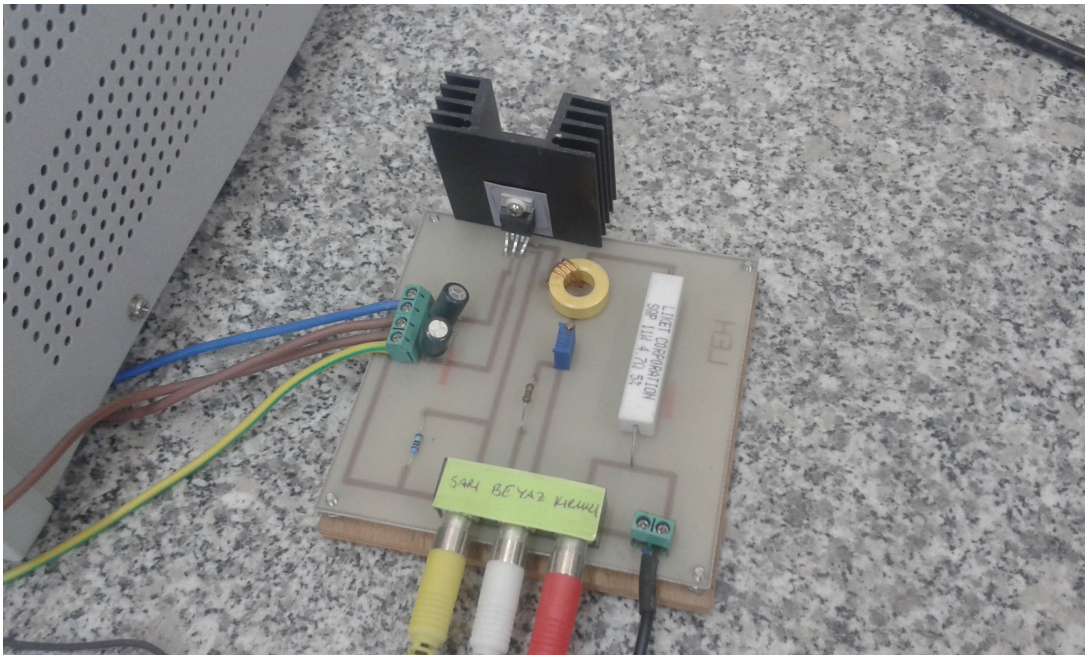

Figure 2.9: Circuit used in the 3ω setup

is made of nickel and its properties are given in Table 2.2.

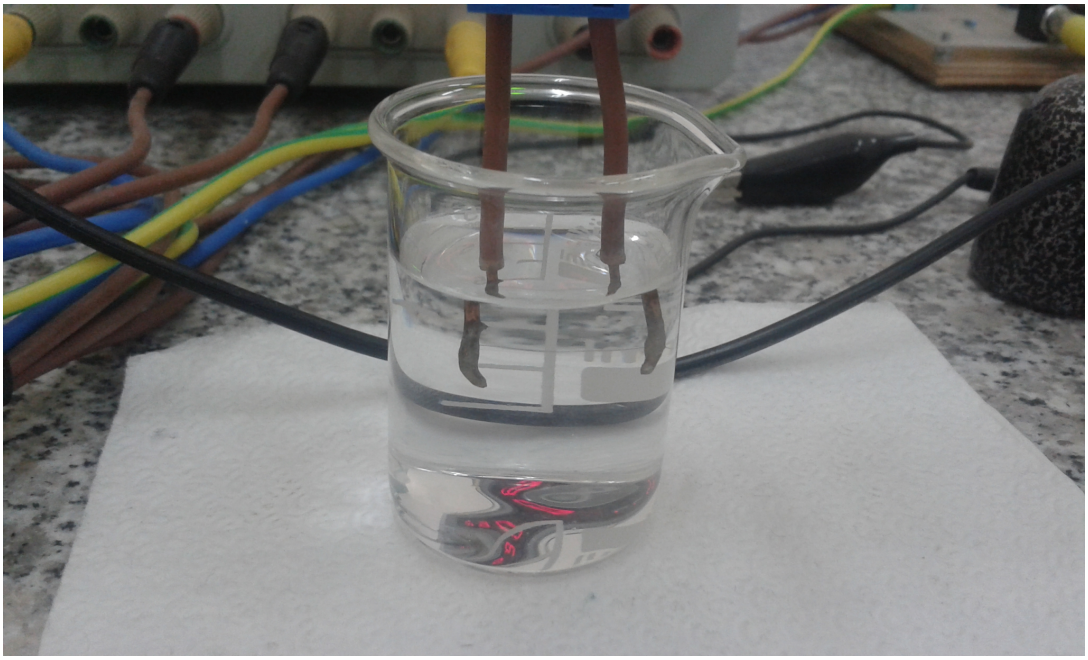

Figure 2.10: Hot wire of the 3ω setup

For the setup used, temperature oscillations are set to approximately 1.25 °C, for which convection effects can be neglected. The sine wave frequency is set to 0.5 Hz, for which the setup is shown to give reliable results [46].

Table 2.2: 3ω method wire properties

Diameter	40 µm
Length	27.94 mm
Thermal conductivity, W/m·K	90.9
Temp. coeff. of resistance, $°C^{-1}$	5.19×10^{-3}

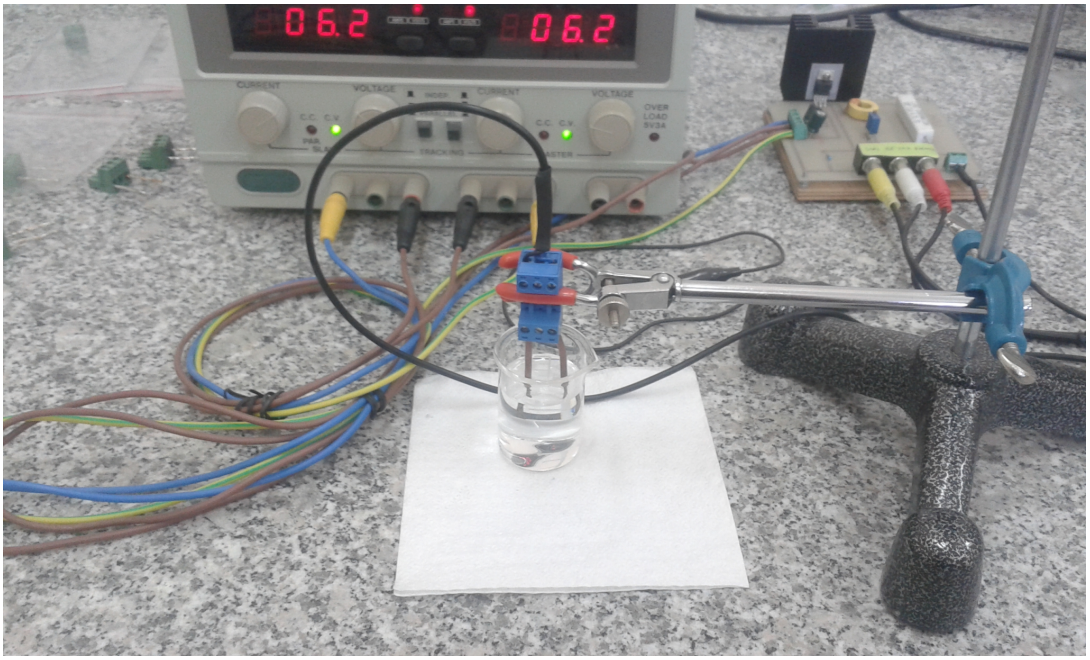

Figure 2.11: 3ω experimental setup

A picture of the entire setup (excluding the lock in amplifier) is given in Figure 2.11.

2.3 Viscosity measurements

The viscosity of the samples have also been measured in this work. Measurements were carried out in Assoc. Prof. Dr. Alpaslan Turgut's laboratory in Mechanical Engineering Department of Dokuz Eylül University. The device used is an A&D SV-10 vibro viscometer (Figure 2.12).

The vibro viscometer measures the viscosity with two thin gold plates that are embedded into the sample. These gold plates are vibrated by an electromagnetic

Figure 2.12: A&D SV-10 vibro viscometer

force at a constant frequency but in reverse phase. The amplitude of this vibration is also kept constant; therefore, by measuring the current that will generate the required force, viscosity is found. The device also has a temperature sensor since the viscosity is strongly dependent on temperature. The device is also capable of measuring the viscosity at different temperatures by embedding the sample in a water jacket. Water in the jacket is circulated by a temperature controllable water circulator (Figure 2.13).

Figure 2.13: Constant temperature water provider for viscometer

2.4 Thermal conductivity measurements of powdered GA

A value on the thermal conductivity of GA was not found in the literature. Therefore its conductivity was measured with Shotherm QTM-D2, a conductivity measurement setup based on transient hot wire method (Figure 2.14), in Dokuz Eylül University.

Figure 2.14: Shotherm QTM-D2

2.5 Preparation of nanofluids

Nanofluids in this work were prepared using the two step method, meaning that the nanoparticles were not synthesized in a chamber containing the base fluid, but were added externally to the base fluid after synthesis. All the work regarding the preparation of nanofluids was conducted in Nanomaterials and Devices Laboratory of Metallurgical and Materials Engineering Department.

CNTs were bought from US Research Nanomaterials, Inc.. The base fluid is deionized water produced by using a Human Corporation Zeener Power water purification system, as shown in Figure 2.15a. The quality of water produced was $18.3 \times 10^6\,\Omega{\cdot}\text{cm}$ [65].

Each sample was produced separately, rather than diluting one large sample. Therefore water, CNT and GA were weighed for every sample (Figure 2.15b).

Nanofluid preparation starts by adding the CNTs in water. Since CNTs will either stay on the surface of the water or completely sink to the bottom, the

(a) Zeener Power water purifier

(b) Axis AGN220C professional balance

(c) Ultrasonic cleaner

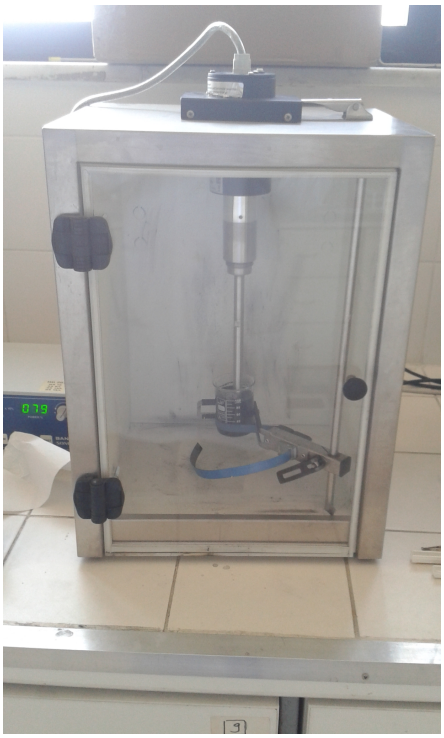

(d) Bandelin Sonopuls HD2070 probe sonicator

Figure 2.15: Instruments used in nanofluid preparation

mixture is sonicated in ultrasonic bath for 5 minutes (Figure 2.15c). Temperature of the bath is set to 33°C. After the 5-minute sonication, GA is added to the mixture. This mixture is sonicated again in ultrasonic bath for 25 minutes. Finally, the mixture is sonicated in probe sonicator (Figure 2.15d) set to 400 W for 15 minutes. The label and properties of prepared nanofluids are tabulated in Table 2.3. In this table, ϕ_{rat} denotes the volumetric concentration ratio of GA to that of CNT.

Table 2.3: Properties of prepared nanofluids

Sample	CNT Type	d_{CNT}(nm)	ϕ_{CNT} (%)	ϕ_{GA} (%)	ϕ_{rat}
A1	MW	<7	0.024	0.009	0.375
A2	MW	10-20	0.024	0.009	0.375
A3	MW	10-20	0.012	0.005	0.417
A4	MW	10-20	0.006	0.002	0.333
A5	MW, short	10-20	0.024	0.009	0.375
A6	DW	2-4	0.024	0.009	0.375
A7	MW, short	10-20	0.024	0.009	0.375
A8	SW	1-2	0.024	0.009	0.375
B1	MW	<7	0.476	0.361	0.758
B2	MW	<7	0.472	0.178	0.377
B3	MW	<7	0.481	0.074	0.154
B4	MW	<7	0.476	0.036	0.076
B5	MW	<7	0.237	0.356	1.502
B6	MW	<7	0.239	0.180	0.753
B7	MW	<7	0.240	0.090	0.375

When the sample series B is considered, it should be noted from Table 2.3 that samples B1–B4 have about the same ϕ_{CNT} but decreasing ϕ_{GA}. Likewise, samples B5–B7 follow the same trend for the purpose of comparison.

The nanofluids were initially prepared on a mass basis, however, the convention in the literature is to use volumetric concentration. Therefore, true densities of CNT and GA are needed to convert the masses into volume. The density of a single nanotube, ρ_{CNT} is taken as 2.1 g/cm^3, as stated in manufacturer's product

specifications [66]. True density of GA, ρ_{GA}, is taken as $1.4\,g/cm^3$ [67], it should be kept in mind that this may not be the exact value for the GA used in this work. These values are also used as input parameters of the models in Section 4.4.

Sample series A have been produced with the help of Dr. Mostafa Kahani, who has worked as a post graduate fellow at METU. Sample series B have later been produced with higher concentrations. About 7 months after their preparation, the TEM images of sample B5 were taken (Figure 2.16).

TEM images reveal that contrary to product specifications, these nanotubes are shorter and have higher diameters. From the images, the diameter and lengths of CNTs were found to range from 10 nm to 36 nm and 0.3 µm to 3 µm, respectively. The use of probe sonicator is believed to break the longer tubes into shorter ones. Due to the GA layers around the CNTs, it is challenging to estimate the exact diameter. For the models, the diameter and the length of nanotubes are taken from the images.

GA can also be seen from the TEM images. The marked region in Figure 2.16b is GA layered around the CNTs. It is not possible, however, to deduce the thickness of this layer from the images because it is not clear from the images where the GA layer starts from. It can also be seen from Figure 2.16d that there is GA that is not adhered on the surface of CNTs.

2.5.1 Uncertainty analysis of nanofluid preparation

Most of the uncertainty in the experimental method comes from the nanofluid preparation step. CNTs were difficult to transfer from their package to the beaker, while weighing on the balance between the transfer. Therefore, some of the CNTs were spilled around during the process.

Figure 2.17 depicts the spilling during weighing. This photograph shows the highest amount of spillage, during both CNT and GA weighing. The paper used to put the CNTs on are a standard paper; using a larger paper to avoid spilling would not fit into the balance. Visual inspection of the picture reveals

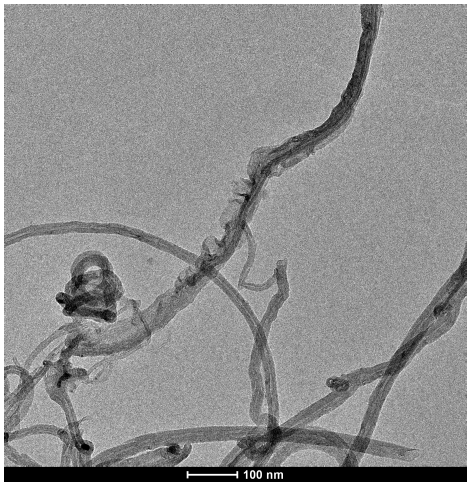

(a) TEM image 1

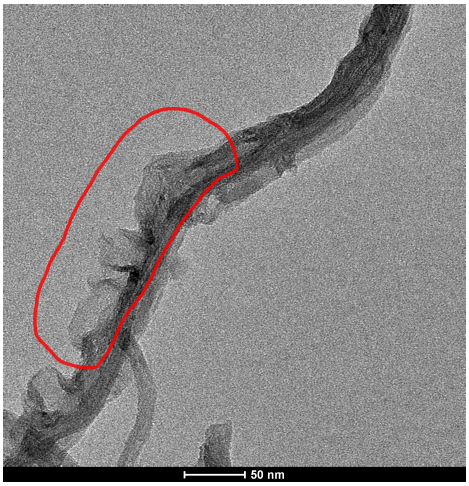

(b) TEM image 2

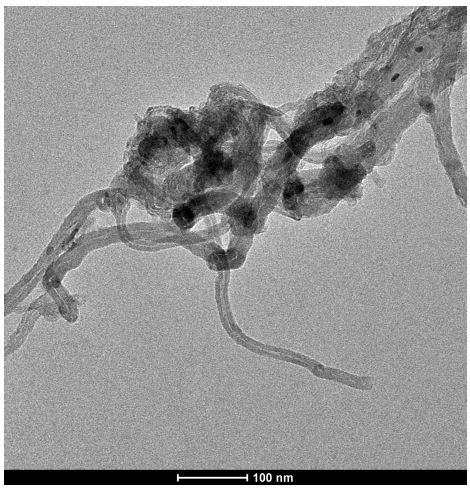

(c) TEM image 3

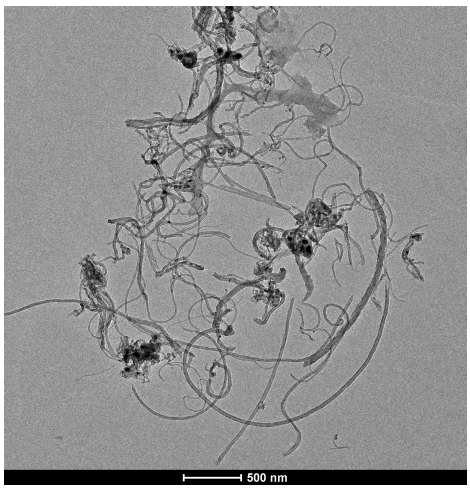

(d) TEM image 4

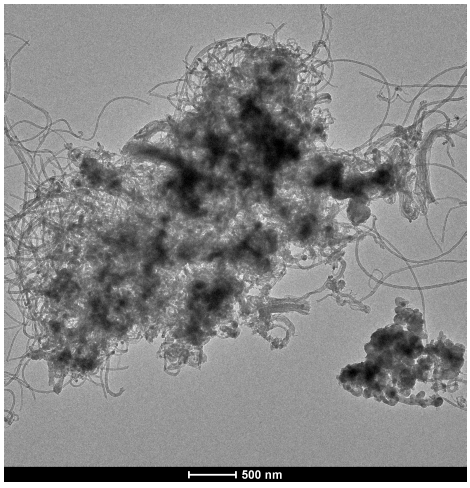

(e) TEM image 5

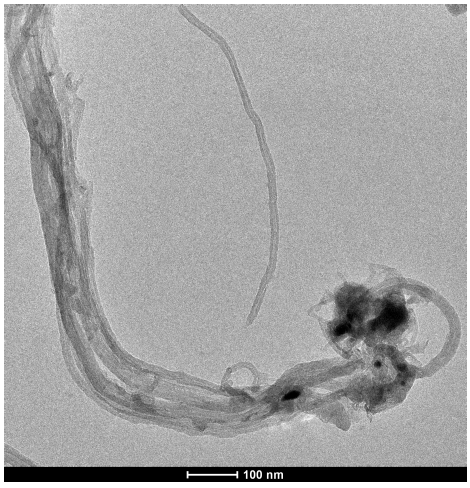

(f) TEM image 6

Figure 2.16: TEM images of Sample B5

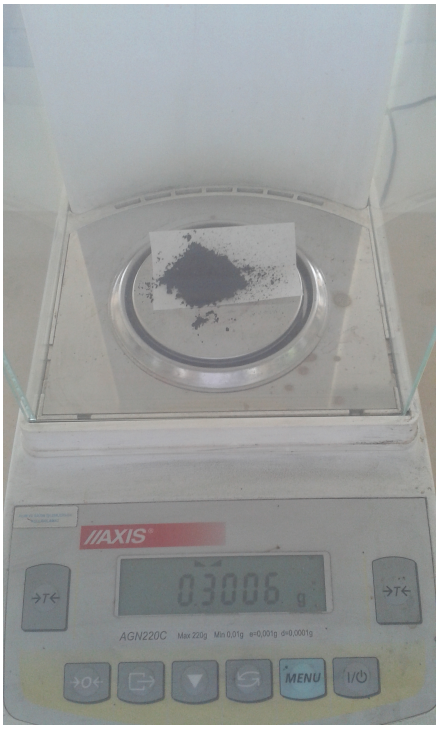

Figure 2.17: Spilling of CNTs during weighing

that about 5% of the total CNT was spilled. This spilled portion from now on will be referred to as spill factor, denoted by f_s. The mass of particle (either CNT or GA) in the nanofluid, m_{p} can be expressed in terms of measured particle mass, $m_{\mathrm{p,meas}}$,

$$m_{\mathrm{p}} = (1 - f_s) m_{\mathrm{p,meas}} \tag{2.14}$$

therefore the uncertainty in CNT amount in the nanofluid, $u_{m_{\mathrm{p,NF}}}$, can be written as follows;

$$u_{m_{\mathrm{p}}} = \sqrt{\left(\frac{\partial m_{\mathrm{p}}}{\partial f_s} u_{f_s}\right)^2 + \left(\frac{\partial m_{\mathrm{p}}}{\partial m_{\mathrm{p,meas}}} u_{m_{\mathrm{meas}}}\right)^2} \tag{2.15}$$

where $u_{f_s} = 0.05$ and $u_{m_{\mathrm{meas}}}$ is the uncertainty of mass measurement of the electronic balance, which is 0.1 mg.

There was no spillage of water, therefore the uncertainty in water mass, $u_{m_{\mathrm{water}}} = u_{m_{\mathrm{meas}}}$.

Mass concentrations of CNT and GA are given by the formula,

$$\gamma_{\mathrm{p}} = \frac{m_{\mathrm{p}}}{m_{\mathrm{NF}}} \tag{2.16}$$

where m_{NF} is the total mass of the nanofluid. Thus the uncertainty in mass concentration is given by the formula,

$$u_{\gamma_{\mathrm{p}}} = \sqrt{\left(\frac{\partial \gamma_{\mathrm{p,NF}}}{\partial m_{\mathrm{p}}} u_{m_{\mathrm{p,NF}}}\right)^2 + \left(\frac{\partial \gamma_{\mathrm{p,NF}}}{\partial m_{\mathrm{NF}}} u_{m_{\mathrm{NF}}}\right)^2} \tag{2.17}$$

where

$$m_{\mathrm{NF}} = m_{\mathrm{water}} + m_{\mathrm{CNT}} + m_{\mathrm{GA}} \tag{2.18}$$

and

$$u_{m_{\mathrm{NF}}} = \sqrt{u^2_{m_{\mathrm{water}}} + u^2_{m_{\mathrm{CNT}}} + u^2_{m_{\mathrm{GA}}}} \tag{2.19}$$

Volumetric concentration of the particles can be expressed as follows;

$$\phi_{\mathrm{p}} = \frac{m_{\mathrm{p}} \rho_{\mathrm{NF}}}{m_{\mathrm{NF}} \rho_{\mathrm{CNT}}} = \frac{\rho_{\mathrm{NF}}}{\rho_{\mathrm{CNT}}} \gamma_{\mathrm{p}} \tag{2.20}$$

where density of the nanofluid is assumed to be equal to the density of water, $1\,\mathrm{g/cm^3}$, which is a reasonable assumption considering the density of CNT and GA and their low concentrations. With $\rho_{\mathrm{CNT}} = 2.1\,\mathrm{g/cm^3}$, the uncertainty in ϕ_{p} is given as

$$u_{\phi_{\mathrm{p}}} = \frac{1}{\rho_{\mathrm{p}}} u_{\gamma_{\mathrm{p}}} \tag{2.21}$$

Detailed composition of nanofluids and uncertainties in their volumetric concentration are given in Table B.1. The uncertainty values are given as percentages.

The average uncertainty in volumetric concentration is estimated to be about 5%, which is predominantly due to spill factor.

Up until now the calculation of uncertainty in volumetric concentration was due to assesable sources of errors. However, there could have been other sources of errors which were very difficult to include in the uncertainty calculations. For example, each time a nanofluid was transferred from a beaker to another, there would be residual CNTs adhered on the beaker, which would mean a decrease in the sample's volumetric concentration. This factor is negligible for sample series A, due to their very low concentrations, but for sample series B, the adhesion is quite observable, especially for samples with lower GA concentrations, like sample B4, as can be seen in Figure 2.18. These photographs were taken during the transfer of samples from their containers to the container of Dr. Turgut's thermal conductivity measurement setup. Figure 2.18 also depicts the effect of GA; sample B4 (Figure 2.18b) had the least amount of GA in the B series, while B5 (Figure 2.18c) had the most.

(a) Sample B3 (b) Sample B4 (c) Sample B5

Figure 2.18: Adhesion of CNTs on beakers

The next chapter presents the thermal conductivity models used for comparison with the measurement results. These models have been modified to handle the effect of surfactant in different concentrations.

CHAPTER 3

NUMERICAL COMPUTATION OF THERMAL CONDUCTIVITY

As mentioned in Section 2.5, nanofluids in this work contain CNT and GA. Therefore to numerically estimate the thermal conductivity of the nanofluid, a model that deals with two different materials is needed.

For GA to work as a surfactant, it has to adhere on the surface of CNT. Adhesion of GA on CNT was shown in Figure 2.16. Therefore it can be said that a layer consisting of GA molecules is formed around CNTs, and a model that includes layer effects could be suitable for use in this work.

Renovated Maxwell (RM) and renovated Hamilton Crosser (RHC) models are two of the earliest thermal conductivity models derived for nanofluids. They include the effect of nanolayers on their base models. Nanolayer is a layer formed around a nanoparticle that consists of base fluid molecules, as shown in Figure 3.1. Molecules of this layer are more ordered than free liquid molecules, therefore presumed to have higher thermal conductivity.

Not much is known about the thickness and thermal conductivity of nanolayers; therefore these models usually assume these values. However, the present work considers surfactant as the nanolayer, therefore its thermal conductivity and thickness are more predictable.

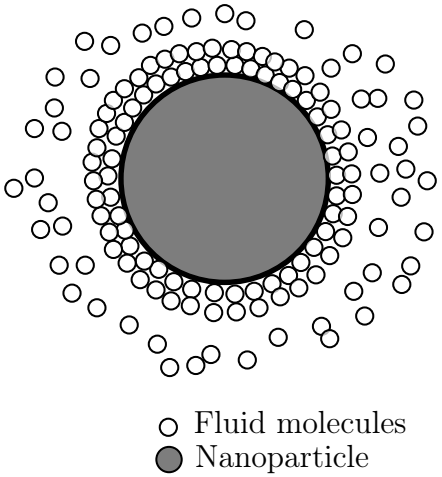

Figure 3.1: Schematic representation of nanolayer

3.1 Renovated Maxwell model

RM model, as the name suggests, is based on Maxwell's model for effective thermal conductivity of heterogeneous mixtures, and is given by the formula [1];

$$k_e = \frac{k_p + 2k_f + 2(k_p - k_f)\phi}{k_p + 2k_f - (k_p - k_f)\phi} k_f \tag{3.1}$$

This model assumes that there is only heat diffusion in the medium, particles are distributed widely enough throughout the medium so that each particle's effect on overall heat flux is independent of each other and particles are spheres of equal diameter.

Yu and Choi's modification of Maxwell's model redefines the particle as a particle-nanolayer composite, with an effective volume concentration and particle thermal conductivity given as follows [48],

$$\phi_e = \phi \left(1 + \frac{h}{r}\right)^3 \tag{3.2}$$

where ϕ is the CNT volumetric concentration, r is the particle radius and h is the thickness of the layer and

$$k_{pe} = \frac{\left[2(1-\nu) + \left(1+\frac{h}{r}\right)^3 (1+2\nu)\right]\nu}{(\nu-1) + \left(1+\frac{h}{r}\right)^3 (1+2\nu)} k_p \tag{3.3}$$

where $\nu = k_l/k_p$.

Thus, by replacing ϕ with ϕ_e and k_p with k_{pe} in Equation 3.1, renovated model is obtained;

$$k_e = \frac{k_{pe} + 2k_f + 2(k_{pe} - k_f)\phi_e}{k_{pe} + 2k_f - (k_{pe} - k_f)\phi_e} k_f \tag{3.4}$$

RM model takes the particles as spheres and uses particle radius as a parameter. Therefore, CNTs will have to be assumed as spherical particles in this model and an effective radius will be calculated by equating its volume to that of a sphere;

$$r_e = \left(0.75 r_{CNT}^2 L_{CNT}\right)^{1/3}. \tag{3.5}$$

The model will also have to be modified to calculate the GA thickness. When all the GA in the nanofluid is assumed to uniformly adhere on CNTs, the layer thickness can be found as

$$h = r_e \left[\left(\frac{\phi_{\mathrm{GA}}}{\phi_{\mathrm{CNT}}} + 1 \right)^{1/3} - 1 \right]. \tag{3.6}$$

RM model used in this work is summarized in the flow chart given in Figure 3.2.

3.2 Renovated Hamilton Crosser model

Similar to the case in Renovated Maxwell model, Renovated Hamilton Crosser model is the updated version of original Hamilton Crosser model that includes nanolayer effects. Hamilton Crosser model is given as follows;

$$k_e = \frac{k_p + (n-1)k_f + (n-1)(k_p - k_f)\phi}{k_p + (n-1)k_f - (k_p - k_f)\phi} k_f. \tag{3.7}$$

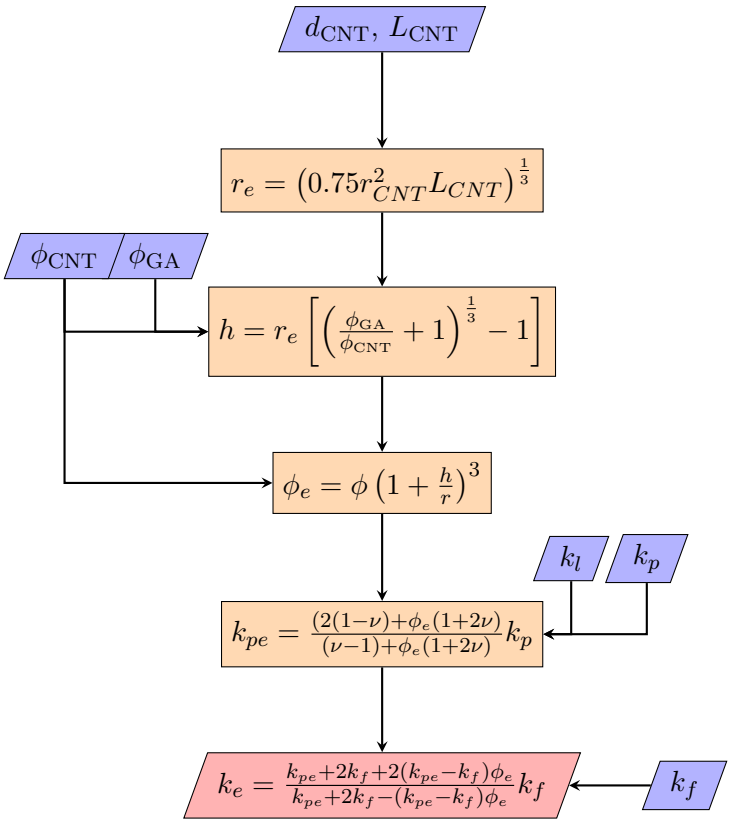

Figure 3.2: Flow chart for Renovated Maxwell model

The shape factor, n, is given by

$$n = \frac{3}{\psi} \tag{3.8}$$

where ψ is the sphericity of the particle, which is defined as ratio surface area of sphere with equal volume of the particle to the surface area of the particle. When $\psi = 1$, in other words, when particles are spherical, Equation 3.7 is reduced to Maxwell model, Equation 3.1.

In RHC model, the layer is assumed to be formed in such a way that bare particle and layered particles are confocal ellipsoids. These two ellipsoids satisfy the following equation:

$$\frac{x^2}{a^2+v} + \frac{y^2}{b^2+v} + \frac{z^2}{c^2+v} = 1 \tag{3.9}$$

where a, b and c are the semiaxes lengths in x, y and z directions, respectively.

Since the thickness of the layer is not constant throughout the surface, the thermal conductivity of the complex ellipsoid will be anisotropic. Therefore the equivalent particle conductivity in the three axes are given as [49]

$$k_{pj} = \left(1 + \frac{k_p - k_l}{k_p\left(n\ d(j,0) - d(j,v)\right) - k_l\left(n\ d(j,0) - d(j,v) - n\right)}\right) k_l \tag{3.10}$$

where j indicates the semiaxes lengths in their respective directions and $d(j,v)$ is the depolarization factor defined as

$$d(j,v) = \frac{\sqrt{(a^2+v)(b^2+v)(c^2+v)}}{2} \times \int_o^\infty \frac{d\eta}{(j^2+v+\eta)\sqrt{(a^2+v+\eta)(b^2+v+\eta)(c^2+v+\eta)}}. \tag{3.11}$$

Equation 3.11 satisfies the condition,

$$d(a,v) + d(b,v) + d(c,v) = 1 \tag{3.12}$$

For spheres, $d(a,v) = d(b,v) = d(c,v) = 1/3$. For prolate spheroids with $a > b = c$,

$$d(a,v) = \frac{1-\epsilon^2}{\epsilon^2}\left[\frac{1}{2\epsilon}\ln\left(\frac{1+\epsilon}{1-\epsilon}\right) - 1\right] \tag{3.13}$$

where ϵ is the eccentricity of the particle. The eccentricity for the particles for this work is given as

$$\epsilon(a,b,v) = \sqrt{1 - \frac{b^2+v}{a^2+v}}. \tag{3.14}$$

Similar to the case in RM model, the effective volumetric concentration of the nanolayer+nanoparticle composite has to be found;

$$\phi_e = \beta\phi \tag{3.15}$$

where β is the volume ratio of the complex ellipsoid to the nanoparticle,

$$\beta = \frac{\sqrt{(a^2+v)(b^2+v)(c^2+v)}}{abc}. \tag{3.16}$$

When k_pe and ϕ_e are found, RHC model can be written [49]:

$$k_e = \left(1 + \frac{n\phi_e A}{1-\phi_e A}\right) k_f \tag{3.17}$$

where A is given by

$$A = \frac{1}{3}\sum_{j=a,b,c} \frac{k_{pj} - k_f}{k_{pj} + (n-1)k_f} \tag{3.18}$$

Yu and Choi argue that, dependance of n on ψ is higher for highly elongated ellipsoids and therefore Equation 3.8 should be modified as follows [49];

$$n = 3\psi^{-\kappa} \tag{3.19}$$

where κ is an empirical parameter depending on particle shape and particle to liquid thermal conductivity ratio. Equation 3.17 uses this generalized shape factor value instead of Equation 3.8.

RHC appears to be more suitable for use in this work because CNTs are cylindrical particles with very high aspect ratios and an ellipsoid with $a >> b = c$ can be taken as a cylinder. This type of ellipsoids are called prolate ellipsoid (or spheroid) and their sphericity can be found as

$$\psi = \frac{2\epsilon(1-\epsilon^2)^{1/6}}{\epsilon\sqrt{1-\epsilon^2} + \arcsin(\epsilon)}. \tag{3.20}$$

A change similar to that in Renovated Maxwell model, Renovated Hamilton Crosser model also requires for the layer thickness to be found from ϕ_{GA}. The thickness parameter, v, is found from the roots of the following equation;

$$v^3 + (a^2 + b^2 + c^2)v^2 + (a^2b^2 + b^2c^2 + a^2c^2)v - \left[2\frac{\phi_{\mathrm{GA}}}{\phi_{\mathrm{CNT}}} + \left(\frac{\phi_{\mathrm{GA}}}{\phi_{\mathrm{CNT}}}\right)^2\right](abc)^2 = 0 \quad (3.21)$$

In Equation 3.21, because the coefficient of v^0 term is always negative and the rest of the coefficients are always positive, only one the roots is definitely positive and the other two are either negative or complex numbers. Therefore the positive root of Equation 3.21 gives the thickness parameter of the layer.

RHC model used in this work is summarized in flow chart given in Figure 3.3.

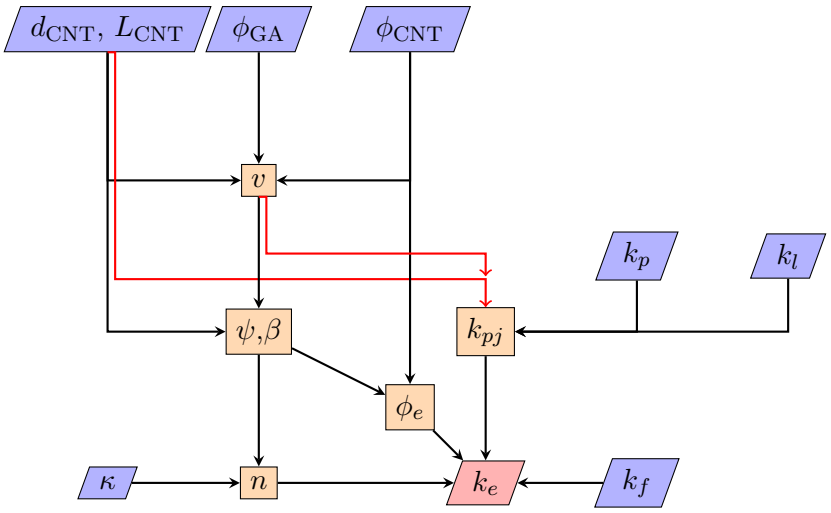

Figure 3.3: Flow chart for Renovated Hamilton Crosser model

3.3 Model validation and initial data

Codes in MATLAB has been developed for the calculations. These codes are initally validated using data from literature before further usage. Figure 3.4 clearly validates that the models were correctly implemented. The solid lines represent the implemented code results and the points are taken from the literature.

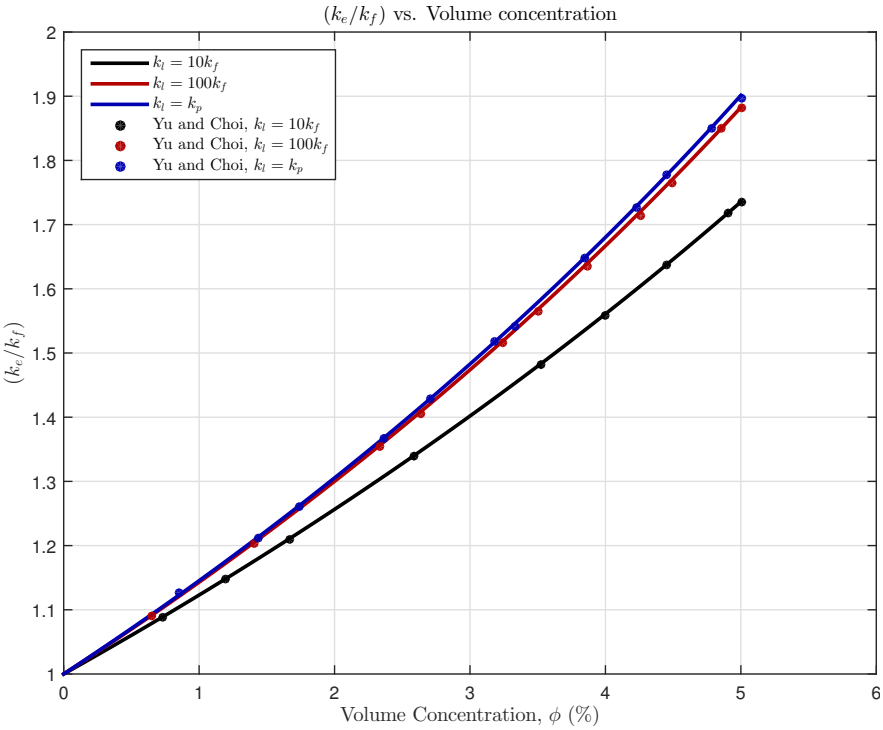

(a) Renovated Maxwell Model

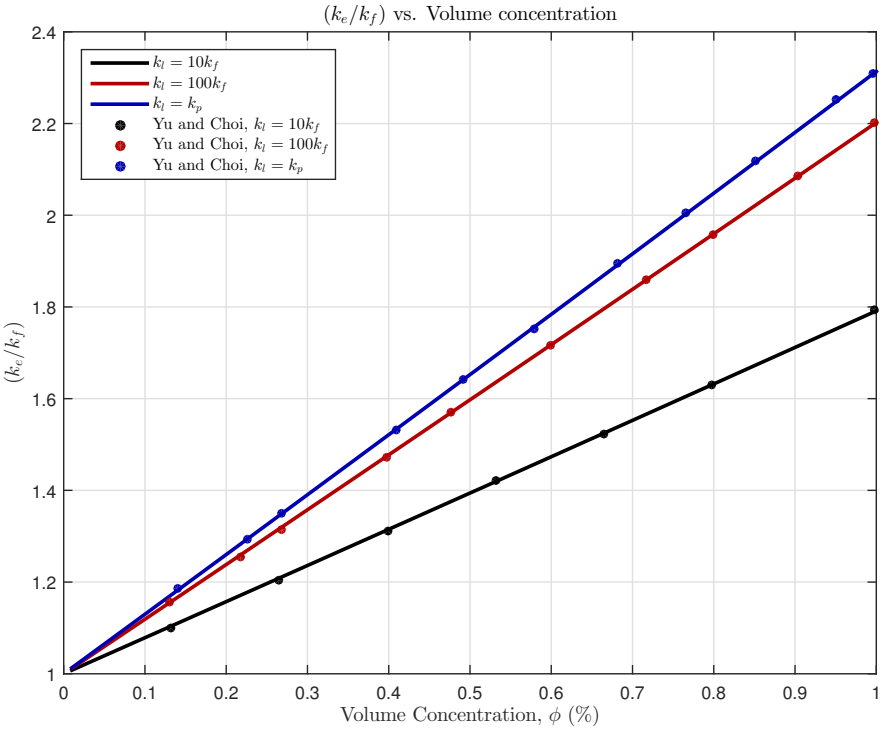

(b) Renovated Hamilton Crosser Model

Figure 3.4: Validation of the models

CHAPTER 4

RESULTS AND DISCUSSION

4.1 Results and discussion of THW experiments

4.1.1 Measurements with the THW setup

The built THW setup was tested with distilled water and EG. Two of the measurements for distilled water are given in Figure 4.1.

The initial 1.5 seconds of Figure 4.1a correspond to the time interval before the switch from the dummy circuit to the main Wheatstone bridge circuit, and therefore should be ignored. This switching portion is trimmed in Figure 4.1b. A glance at both graphs reveals that ΔT starts from a non-zero value. This is because the Wheatstone bridge could be perfectly balanced. Therefore it becomes impossible to deduce the temperature change during the measurement. Also as ΔT decreases, oscillations in the temperature measurement become visible. This is because lower ΔT means lower voltage readings, in which case the noise in the system becomes comparable to the targeted measurement.

Neither first nor the second measurement shows the expected trend; linearity has to eventually disappear due to the emergence of convective effects and axial conduction. According to Kierkus criteria (which will be explained in detail later in section 4.1.4), the interval of measurement for this setup with the thicker wire should be between 2.4 s and 24 s. The first measurement shows a trend that is not linear in this interval, especially in the first 10 seconds. The second measurement is closer to being linear in this interval, although there seems a portion of higher

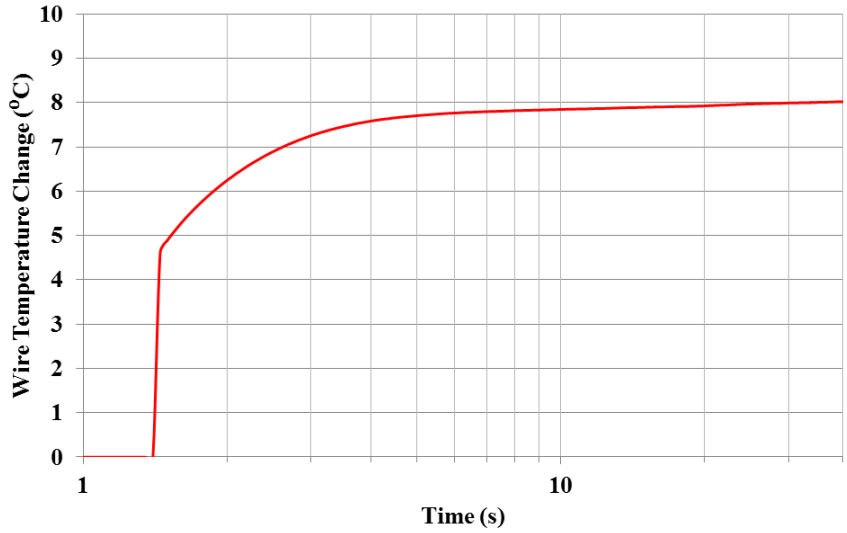

(a) Measurement 1

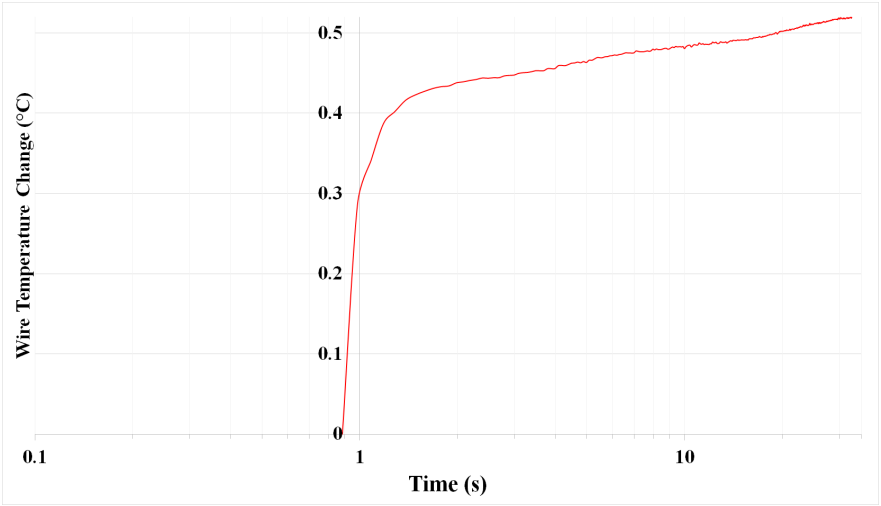

(b) Measurement 2

Figure 4.1: Thermal conductivity measurements of distilled water

slope at the end of the plot, which is the opposite of what is expected.

The slope of the first measurement after about $t = 9\,\mathrm{s}$ gives a thermal conductivity value of $0.56\,\mathrm{W/m\cdot K}$ a value that is close to that of water. This result, however, is shown to be unreliable, because this linear trend is expected to be between $t = 2.4\,\mathrm{s}$ and $t = 24\,\mathrm{s}$, while the slope of the trend is higher and varying for the interval, $1 < t < 9$. This variance is exemplified for measurement 2. Three pairs of points are taken to calculate the slope and hence the thermal conductivity, to check if the sought linear trend is actually inside the interval of

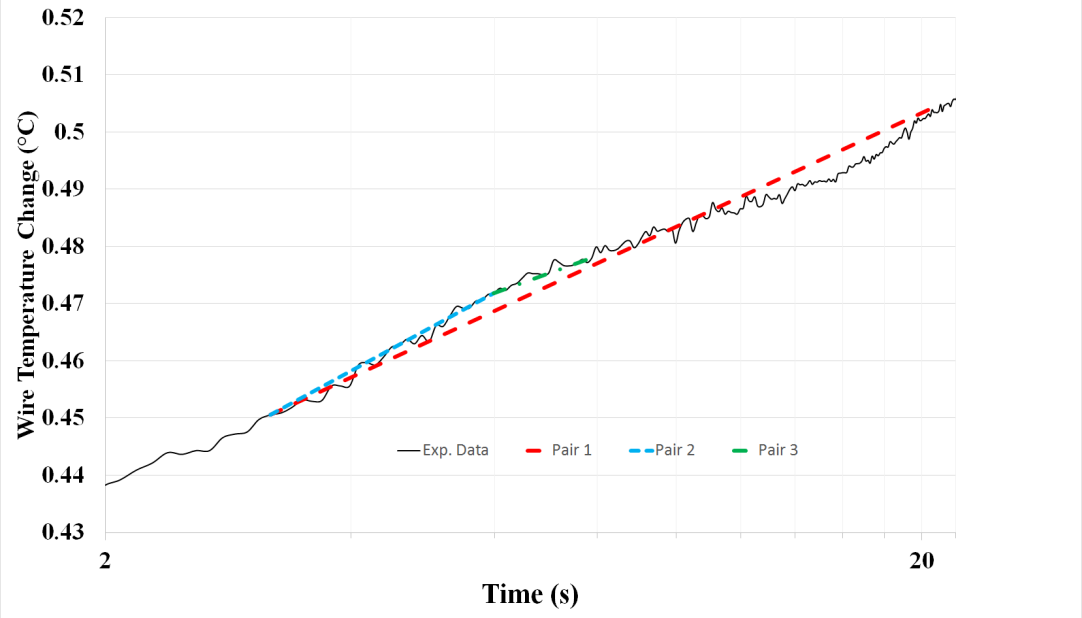

Figure 4.2: Close up view of measurement 2

2.4 s and 24 s. Lines drawn between the pairs can be seen in the close-up view of measurement 2 (Figure 4.2).

Although the slope of these three lines seem slightly different visually, thermal conductivity values differ greatly. This shows that sensitivity of the measurement is too high to obtain reliable results.

It was therefore decided that the reliability of the built setup was inadequate for use in this work and therefore 3ω method was used for the rest of experiments. The measurement results with the 3ω method are presented and discussed in Section 4.2. Following sections discuss the possible sources of errors in the built THW setup.

4.1.2 Wire selection

As stated before in Chapter 2, the wire used in THW method has to be as thin and as long as possible to satisfy one dimensional heat transfer condition. For this reason, the design initially employed a wire with 27.94 µm diameter with only 2.54 µm of it being the coating. With the wire length being 12 cm, this would give an aspect ratio, L_w/r_w, of 8570, which is an acceptable value for

infinitely long line source approximation.

During the construction of the setup and experimental procedure, however, it was found out that the wire was too fragile to handle and too thin to see without any precision equipment. It was especially difficult to tell whether the coating was removed and to what length was it removed, making it uncertain if there is any contact between the bare wire and the sample. For these reasons, on the expense of losing high aspect ratio, a thicker wire was employed. This wire had a diameter of 139.7 µm, with 63.2 µm of it being the coating. This would result in an aspect ratio of 1718. The importance of aspect ratio will be discussed later in Section 4.1.4.

The handling of wire becomes important when maintaining straightness of the wire inside the cell. Wire has to be straight for it to behave as a line source, therefore, while applying little tension from the free end, screws should be tightened to constrain the wire between the aluminum cubes at the same time. There was also the possibility of breaking the wire if cubes were pressed on each other to tight, yet a minimum stress had to be applied otherwise the wire would be loose and therefore lose its straightness. For the constructed setup, this was a delicate balance. Even for the thicker wire, positioning correctly was a difficult task.

Removal of the coating from the tips was a difficult task as well, both for thick and thin wires. Although the coated and uncoated portions of the wires were clearly visible, a controlled removal was not possible, compromising the insulation between the sample and the wire. Also, application of heat could also be resulting in oxidization of platinum or occuring of other changes in the material properties.

4.1.3 Electrical considerations

Although the electrical design of THW method is meant to be simple, some difficulties emerged during the construction of this setup.

The first thing to discuss is the electrical connectivity throughout the circuit. In

the hot wire cell, the electrical path is as follows; copper wire, tightening screw, aluminum cube, platinum wire, aluminum cube, tightening screw and copper wire. Each component is connected by a simple physical touch; copper wires were wound around the screws, screws were touching the cubes by their tips and platinum wire was constricted between the aluminum cubes. Contact resistance between each component can change each time the hot wire cell is disassembled and assembled for refilling or changing the wire, which would require calibration every time. These unsecure connections are also susceptible to disturbance during the experiment, which could effectively disturb the measurement.

The next part is the Wheatstone bridge and the resistors. The resistors have to be chosen carefully; high resistance would result in low power dissipation in the platinum wire and therefore should be avoided. However, when the resistance of the other resistors are low, this time, power dissipation, and therefore heating on these resistors occur as well. Initially, resistors used were common resistors, like the ones in 3ω setup (Figure 2.9). However, these resistors could not handle high currents and burned out. Therefore they were replaced with ceramic resistors than can withstand high currents. Although these ceramic resistors could tolerate high currents, they would also – especially the ones with low resistances like $10\,\Omega$ – would heat up. Heating would result in a change of resistance as high as 10%. This will also lead to change in power dissipation across the platinum wire. Therefore, a complex control and measurement system is needed to include the variable resistor resistances and calculations need to be revised to include time dependent power dissipation.

4.1.4 Kierkus criteria

In 1973, Kierkus *et al.* solved the two dimensional (axial and radial) heat transfer problem of a cylinder with finite length and radius immersed in an infinite medium to investigate the effects of finite length and radius for THW method [36]. Extra boundary conditions of this problem were;

$$T = 0,\ z = 0, z = L_w,\ 0 < r < \infty,\ t > 0 \tag{4.1a}$$

$$2\pi r_w k_f \frac{\partial T}{\partial r} + \pi {r_w}^2 k_w \frac{\partial^2 T}{\partial z^2} + \pi {r_w}^2 \rho_w c_w \frac{\partial T}{\partial t} = -Q,$$

$$r = r_w,\ 0 < z < L_w,\ t > 0. \quad (4.1b)$$

Equation 4.1a means that the two ends of the cylinder are at constant temperature with $T = 0$ and Equation 4.1b indicates a uniform heat generation on the surface of the cylinder. The authors solved this problem for various values of dimensionless parameters, L_w/r_w, $(\rho_f c_f)/(\rho_w c_w)$ and k_f/k_w with that of the solution of the ideal case.

The authors state that, in order to use in a THW setup, following criteria should be met for acceptable error ranges;

$$\sqrt{\frac{\rho_f c_f}{\rho_w c_w}} \frac{L_w}{r_w} > 500 \quad (4.2a)$$

$$\sqrt{\frac{k_f}{k_w}} \frac{L_w}{r_w} > 500 \quad (4.2b)$$

$$100 < \frac{k_f t}{\rho_w c_w {r_w}^2} < 1000. \quad (4.2c)$$

The first two criteria require as high aspect ratio as possible. The third criterion is about the measurement time; temperature measurement of the sample must be performed during the specified interval.

The Kierkus criteria mean that the thermal conductivity of some liquids may not be measurable with certain setups due to the length, diameter and material properties of the wire, but by increasing the aspect ratio, a wider range of liquids can be measurable.

The setup built in this work was intended to be used mainly to measure water based nanofluids. No matter what particles are used, the resulting nanofluids' thermal properties are expected to be close to its base fluid; water due to low particle concentrations. Therefore, checking whether this setup meets the Kierkus criteria is done by considering the properties of water and platinum, which are given in Table 4.1.

Table 4.1: Material properties of water and platinum

Data	Water	Platinum
Density, ρ (kg/m^3)	1000	21450
Heat capacity, c (kJ/kg·K)	4.18	0.133
Thermal conductivity, k (W/m·K)	0.6	71.6

With the values from Table 4.1, the first wire satisfied the first two criteria. However, according to the third criterion, measurement must be taken between 0.0092 s and 0.92 s, which is not a practical interval considering the setup. The thicker wire fails to meet the second criterion. The wire length had to be at least 39 cm to satisfy this criterion. Eventually, both wires were found unsuitable for use in the current setup. Hot wire cell design should be revised and its length increased such that thicker wire can be used while satisfy all criteria.

4.2 Results from the 3ω experiments

4.2.1 Thermal conductivity enhancement

Thermal conductivity results from the measurements made on sample series B are tabulated in Table 4.2 and plotted in Figure 4.3. For sample series A, there was no observable thermal conductivity enhancement, most probably due to very low volumetric concentrations.

The results show a proportionality between the volumetric concentration of CNT and thermal conductivity, as expected. The maximum thermal conductivity enhancement has been observed as 3.5% with sample B3 ($\phi_{\mathrm{CNT}} \approx 0.5\%$).

Normally, we would expect GA to decrease the overall thermal conductivity of the nanofluid since its thermal conductivity is less than both that of CNT and water. However, Figure 4.3b depicts some unexpected outcomes when the result for sample B4 is considered. For samples with higher ϕ_{CNT} (marked with black) if the first datum (sample B4) is omitted, the overall thermal conductivity seems to decrease with increasing GA concentration. The omittance of B4 is a

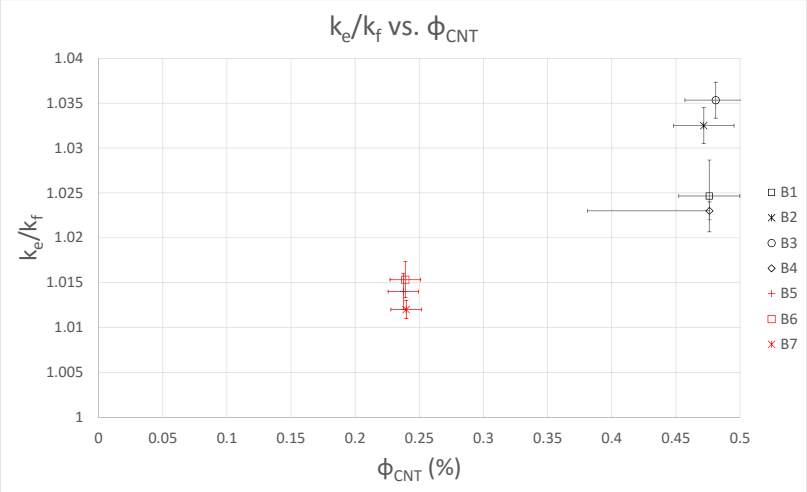

(a) k_e/k_f vs. ϕ_{CNT}

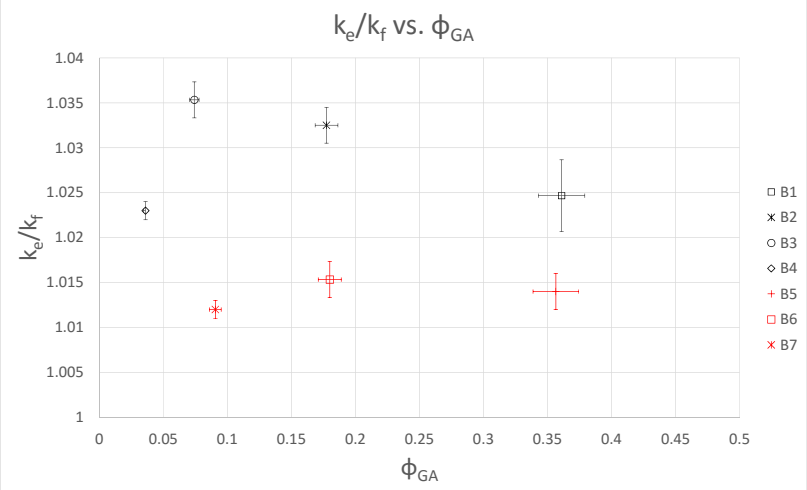

(b) k_e/k_f vs. ϕ_{GA}

Figure 4.3: Thermal conductivity enhancement in sample series B

reasonable practice, considering the unreliability in its volumetric concentration (see Figure 2.18b). A stable solution could not be obtained for this particular

sample most probably due to the very low GA concentration, therefore the real CNT concentration during the measurement was lower than its intended concentration. Moreover, during measurements, possible precipitation of CNT would result in a lower local concentration in the vicinity of the wire, which could also effect the result. As a final remark, it should be noted that the thermal conductivities of the samples have been measured about one month after their preparation. This is quite long considering the published experimental results in the literature.

Table 4.2: Thermal conductivity measurements of sample series B

Sample	Thermal conductivity enhancement, k_e/k_f				
	Meas. 1	Meas. 2	Meas. 3	Meas. 4	Average
B1	1.028	1.025	1.021		1.025 ±0.004
B2	1.030	1.033	1.035	1.032	1.033 ±0.002
B3	1.034	1.035	1.037		1.035 ±0.002
B4	1.023	1.022	1.024		1.023 ±0.001
B5	1.012	1.014	1.016		1.014 ±0.002
B6	1.017	1.014	1.015		1.015 ±0.002
B7	1.013	1.011	1.012		1.012 ±0.001

4.2.2 Comparison with literature

Experimental results have been compared to some of the literature results in Figure 4.4. All these measurements, except for sample series B, Xie *et al.* [22] and Choi *et al.* [44], use a commercial thermal conductivity measurement device named KD2 Pro, a device that is based on THW method. Xie *et al.* uses a custom built THW setup while Choi *et al.* uses a setup based on 3ω method. Data shown in red use GA as surfactant. Data shown in black use a surfactant different than GA, or not stated.

As can be seen from Figure 4.4, the thermal conductivity enhancement in sample series B is below of most data in the literature. One reason is the use of different type of surfactants. However, this explanation alone is not enough, because Ding

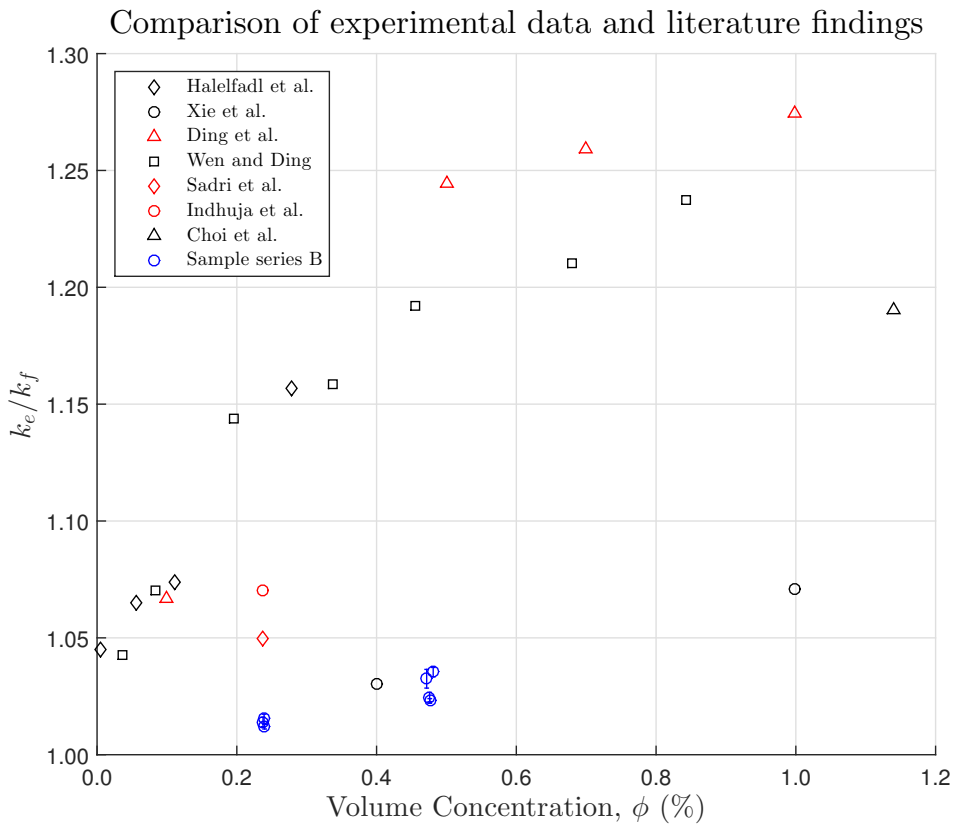

Figure 4.4: Comparison of experimental data and literature findings

et al. also used GA as the surfactant [26], with similar concentrations (0.25% wt.) to sample series B. Another thing to notice is that nanofluids of Xie *et al.* does not contain any surfactant, but CNTs were surface treated with oxygen containing functional groups.

A more convincing explanation can be the agglomeration of particles; the TEM images in Figure 2.16 depict great amount of agglomeration in the samples used in this work, while the TEM images from the literature show good dispersion of nanotubes (see Figure 4.5b). This explanation is further supported by the fact that compared to the samples from the literature, sample series B were sonicated for a very short time. Both Ding *et al.* and Wen and Ding's samples were sonicated for 24 hours [25, 26], while all the samples prepared in this work were sonicated for a total of 40 minutes. The TEM images of sample B5 and Wen and Ding are given in Figure 4.5.

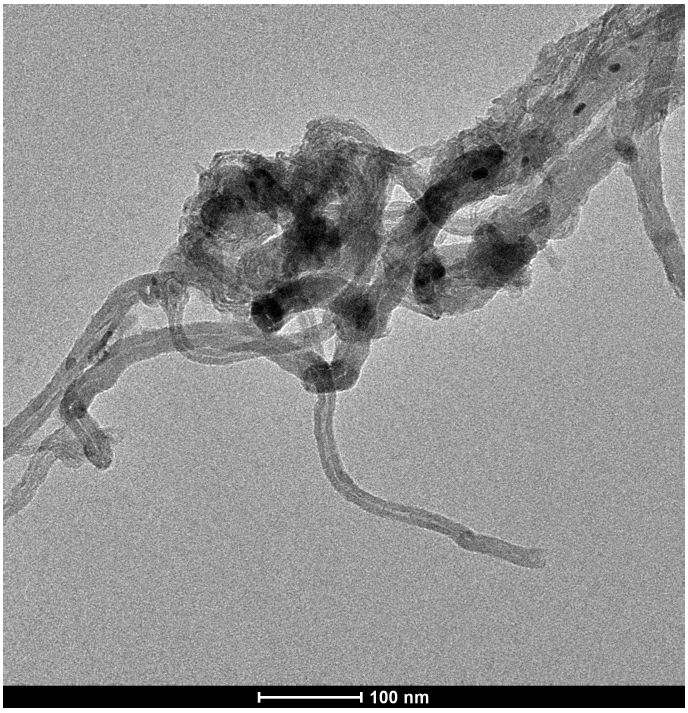

(a) Sample B5

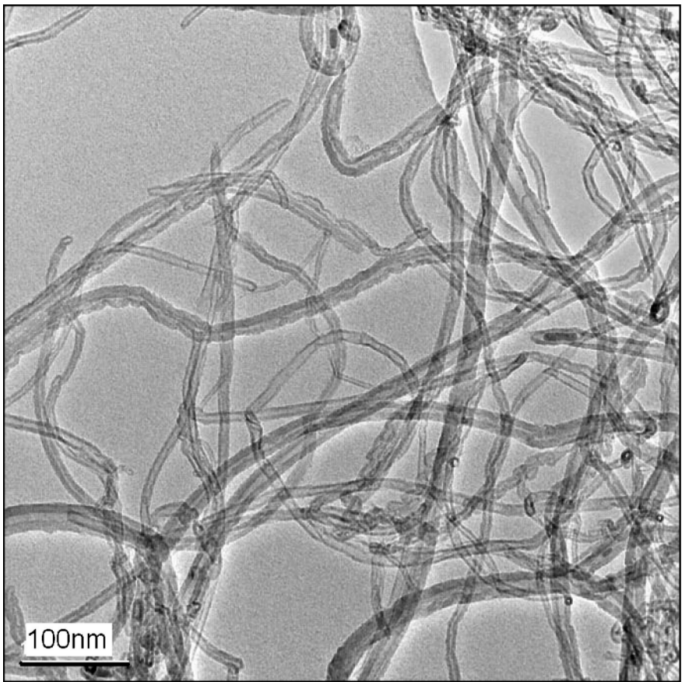

(b) Wen and Ding [25]

Figure 4.5: TEM image comparison

4.3 Viscosities of the samples

Results of viscosity measurements for sample series B are given in Table 4.3. Results of sample series A were not shown because measurement indicate no change in viscosity, which is most probably due to very low concentrations.

Table 4.3: Viscosity measurements of sample series B

Sample	Temperature (°C)	μ (mPa·s)	$\mu_{\mathrm{nf}}/\mu_{\mathrm{f}}$
B1	25.5	1.22	1.39
B2	25.7	1.15	1.32
B3	25.8	1.50	1.72
B4	25.7	2.50	2.85
B5	25.9	1.04	1.19
B6	26.2	1.04	1.20
B7	26.2	0.98	1.13

The viscosity measurements serve the purpose to show that there is indeed CNT in the mixture and its presence can be detected. Although sample series A are also black, that is the only proof of existence of CNT in the water. However for sample series B, increased viscosity is a sign of nanoparticle presence as well, which makes the samples have more characteristics of nanofluids rather than being a water with changed color.

Again, sample B4 has the highest error in terms of ϕ_{CNT} and ϕ_{GA} estimation. Clearly, lower ϕ_{CNT} (B5-B7) yielded lower viscosity as expected. However, it is difficult to talk about a trend with respect to ϕ_{GA} at constant ϕ_{CNT}.

There was not enough data in the literature for comparison, except for the findings of Sadri *et al.* [30]. Their work investigated the effect of sonication times on viscosity and conductivity of nanofluids with 0.5% mass concentration of MWCNT and 0.25% of GA, that is equivalent of sample B6 of this work. For a sonication time of 15 minutes, they found viscosity of the nanofluid at 30 °C as 1.15 mPa·s. Their results seems slightly higher than the findings of this work. A possible explanation for this difference could be the fact that samples of

this work sonicated with a probe sonicator only once during their preparation. Sadri *et al.* also reports that increased sonication time decreases the viscosity, a finding which further supports this argument.

4.4 Results from the models

4.4.1 Effect of particle thermal conductivity

The average radius and the length of the nanotubes have been taken as 10 nm and 1 µm, respectively. These values have been obtained from the TEM images of the samples.

For the RM model, from Equation 3.5, the average equivalent particle radius was found as 42.17 nm.

The thermal conductivity of a nanotube, k_{CNT} is taken as 2000 W/m·K. This is the value that Choi *et al.* take in their calculations and experiments [21, 49], although the exact value of thermal conductivity of carbon nanotubes is still unknown. Therefore, before taking the nanotube conductivity as 2000 W/m·K, both RM and RHC models were run for k_p values ranging from 500 to 10 000 W/m·K, with the upper limit being the highest reported thermal conductivity value for CNTs; a theoretical value for SWCNT above room temperature [68]. As can be seen from Figure 4.6, for the scope of this work, a precise value for k_p is not necessary, therefore k_p can be easily taken as 2000 W/m·K.

The thermal conductivity of GA has been taken as $k_l = 0.1$ W/m·K from the measuremets. It should however be noted that this value is for powdered GA and will most probably change when GA is dissolved in water and later surrounds the particles. This effect is further detailed in Section 4.4.4. All the GA in the mixture is assumed to have adhered uniformly around CNTs.

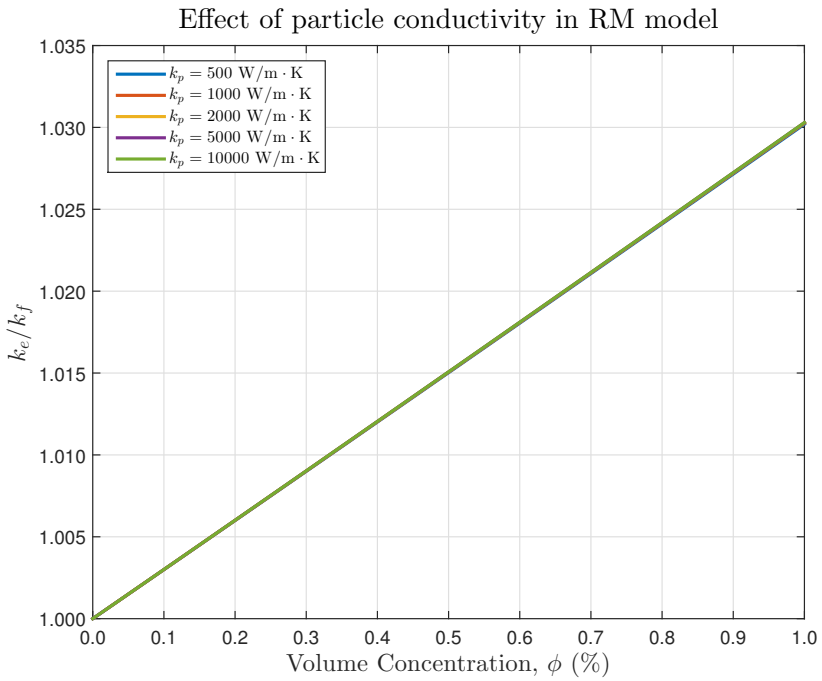

(a) Renovated Maxwell Model

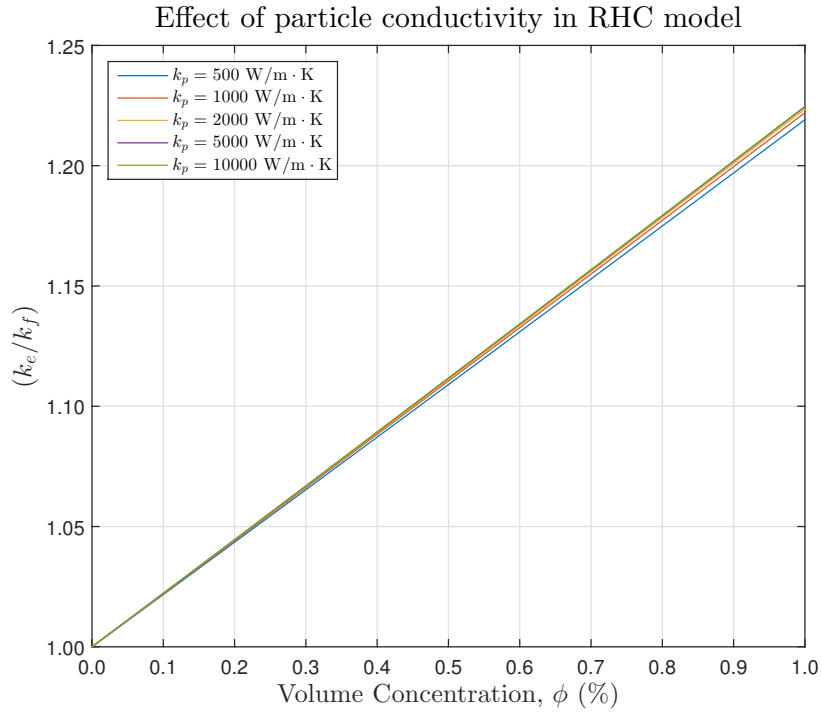

(b) Renovated Hamilton Crosser Model

Figure 4.6: Effect of k_p on thermal conductivity enhancement according to Renovated Maxwell and Hamilton Crosser models

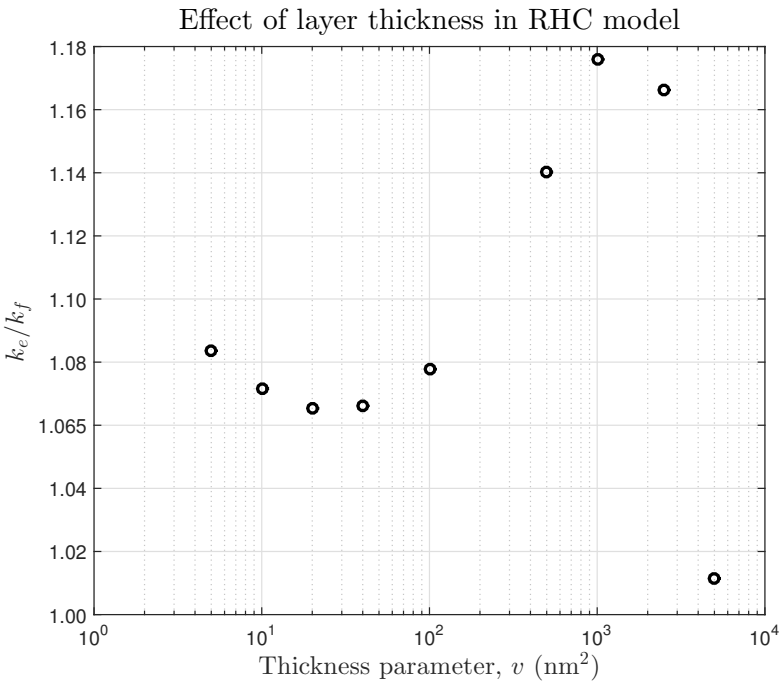

Figure 4.7: Effect of layer thickness in RHC model

4.4.2 The effect of the layer thickness

The mathematical explanation for the irregular behavior of RHC model in response to GA concentration, hence the layer thickness, can be made as follows; for smaller k_{GA}, with an increasing v (parameter associated with GA layer thickness), the effective particle thermal conductivity, k_{pj} (Equation 3.10) is always decreasing. On the other hand, an increase in v means an increase in volume ratio, β, therefore an increase in effective volumetric concentration, ϕ_{e} (Equation 3.15). After a number of test runs, it has been found out that until a very small certain v value, which is roughly around $20\,\mathrm{nm}^2$, the decrease in k_{pj} is faster than the increase in ϕ_e, resulting in a decrease in overall conductivity (Equation 3.17). After $v = 20\,\mathrm{nm}^2$, ϕ_e becomes more effective than k_{pj}, resulting in an increase in overall conductivity. The model eventually starts to give lowered conductivity with increasing GA content, as it physically should be the case, however, this response is not observed until very large v values, v values obtainable when GA content is few hundred times higher than CNT, which is unreasonable. This trend is plotted in Figure 4.7.

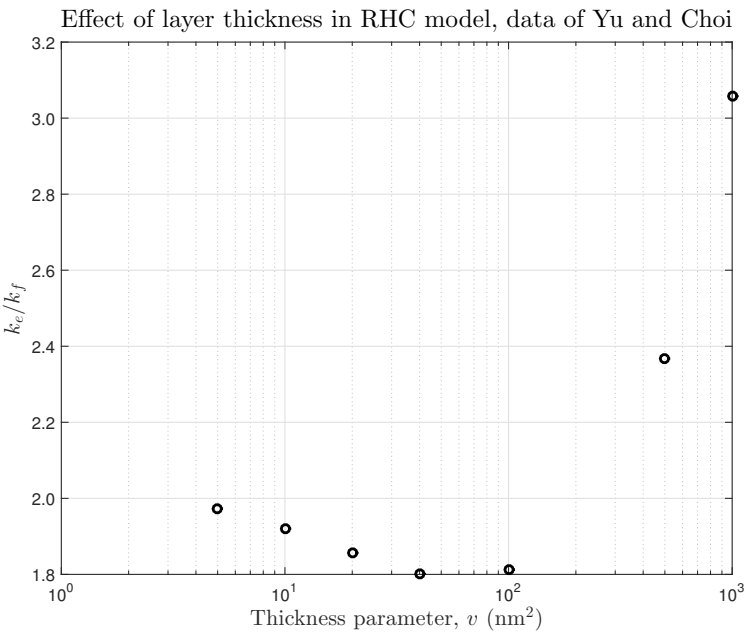

Figure 4.8: Effect of layer thickness, for Yu and Choi's experimental data [49]

These test runs were also conducted for the particle data from the paper of Renovated Hamilton Crosser model [49], with $k_l = 10k_f$. Their particle also demonstrated a decrease in slope of k_e/k_f until $v \approx 100\,\text{nm}^2$ (see Figure 4.8). Decrease in slope disappears for higher layer conductivity, such as $k_l = 100k_f$.

Yu and Choi developed this model with the idea to include the effect of nanolayer, a layer that is argued to enhance the thermal conductivity. Therefore they assume its conductivity to be much higher than the base fluid. This results in a linear proportionality between v and conductivity enhancement for all v. However, for lower layer conductivities, Renovated Hamilton Crosser method proves unsuitable, because there is no reasonable physical explanation for the effect of v on thermal conductivity enhancement.

4.4.3 Effect of empirical parameter, κ

The effect of empirical paramter, κ, on results from RHC model are given in Figure 4.9.

Originally, Hamilton and Crosser used $\kappa = 1.00$ agrees with their experimental

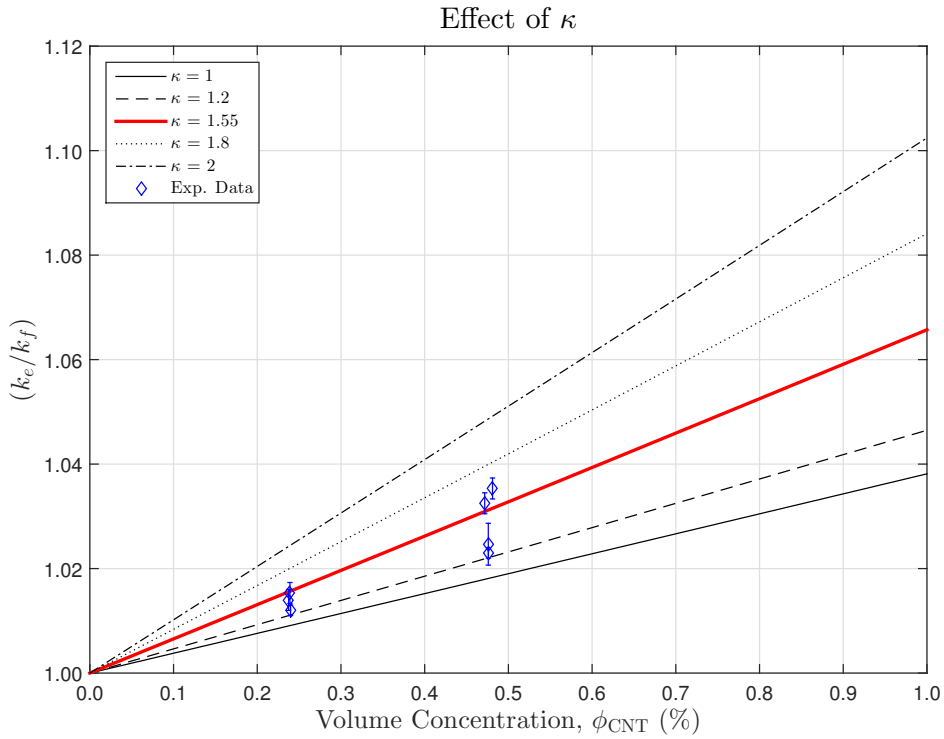

Figure 4.9: Effect of κ on Renovated Hamilton Crosser model

data [47]. Yu and Choi took $\kappa = 1.55$ in their work, because this value fit their experimental data. They argued that such a change in κ for their case is necessary since nanotubes are extremely elongated for direct usage in HC model and the thermal conductivity of particle to liquid is too high. No work on the relation between the particle dimensions and κ was encountered in the literature, therefore this work also took $\kappa = 1.55$. Considering that nanoparticles of Yu and Choi and this work are different, a different value for κ might have been more appropriate. However, because nanotubes in this work are less elongated and ratio of thermal conductivies of particle and base fluid is lower than that of Yu and Choi, κ would be expected to have a value between 1.00 and 1.55. From Figure 4.9, it can be seen that using a κ value between 1.00 and 1.55 would still give results reasonably close to the experimental data. However, an accurate value for κ would be preferable since it has a strong effect on the results.

4.4.4 Effect of layer thermal conductivity

The effect of layer conductivity, k_l for both RM and RHC models can be observed from Figure 4.10.

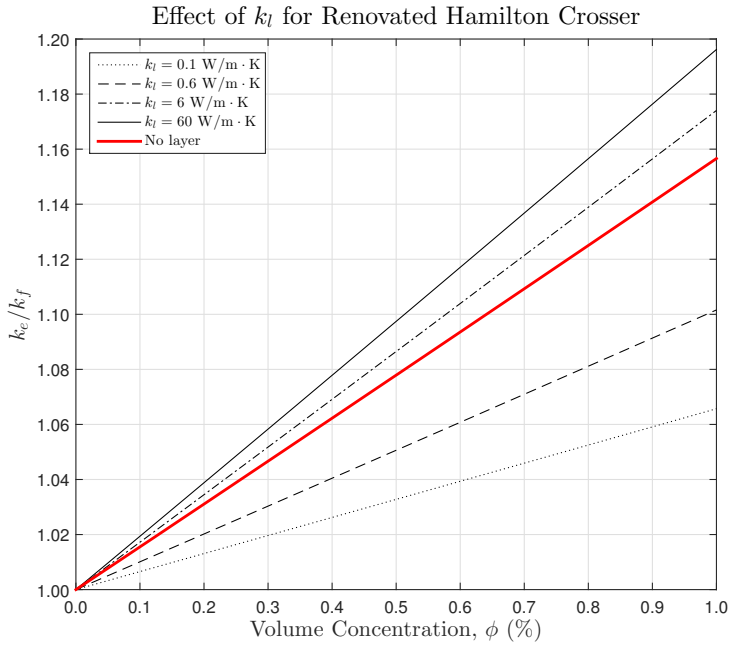

(a) Renovated Hamilton Crosser

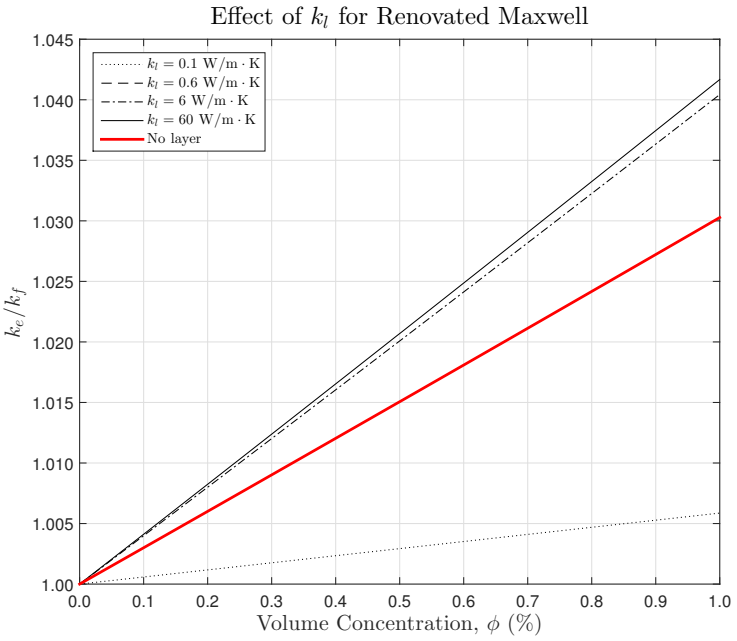

(b) Renovated Maxwell

Figure 4.10: Effect of k_l on nanofluid conductivity

The ratio of ϕ_{GA} to ϕ_{CNT} is the same for all plots and equal to 0.376. Both models show a strong dependence on k_l when k_l is very small compared to k_p and this effect becomes less important as k_l becomes comparable to k_p. This is not surprising since both models use an effective particle thermal conductivity value, the calculation of which is based on averaging the particle properties. What is interesting is while in RM model, $k_l = k_f$ case (0.6 W/m·K) gives the same result as for the case without the layer, RHC model gives two different results for the two mentioned cases. This is most probably caused by the fact that in Hamilton Crosser model, nanoparticle become anisotropic when the layer is formed around it. Since the layer thickness distribution profile is assumed such that the bare particle and coated complex particle are confocal, the amount of layer in different semiaxes directions becomes different, resulting in anisotropy.

If the nanofluid thermal conductivity with the surfactant is to be estimated using these renovated models, one should be very confident in the thermal conductivity value of its surfactant. The surfactant materials would not be expected to have k values comparable to nanofluid nanoparticles, which are usually metals. The effect of k_l would be more dominant if the surfactant concentration were to increase. It is therefore seen again that these models may be good approximations for nanofluid thermal conductivity where the layer is assumed to behave like a thermal bridge, that is, $k_f < k_l < k_p$, but may not be very robust for surfactant modeling.

4.4.5 Effect of CNT dimensions in Hamilton Crosser model

The effect of particle dimensions are investigated for RHC model only because in RM model, particle radius is important only during the effective volumetric concentration, in Equation 3.2. Therefore, examining the effect of particle radius is the same as examining the effect of layer thickness, which has already been done in Section 4.4.2.

In HC model, the affect of aspect ratio of ellipsoids (ratio of axis lengths) was investigated. Results can be seen in Figure 4.11. For the presented results, the empirical parameter is taken as $\kappa = 1.55$ and no surfactant layer has been

considered.

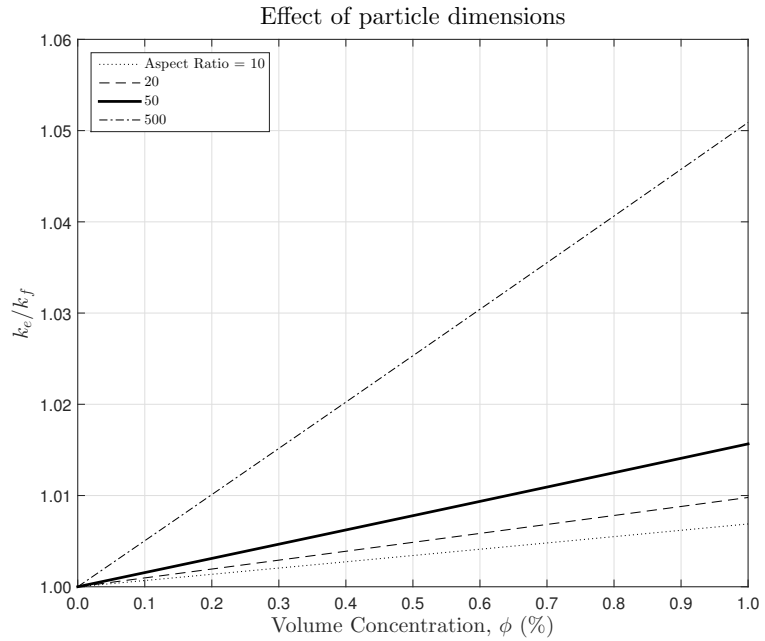

Figure 4.11: Effect of particle dimensions in RHC model

Results from Figure 4.11 reveal that the aspect ratio of ellipsoids greatly influence the overall thermal conductivity of the nanofluid. κ should also be changing, since there is a large difference in the aspect ratio of the results.

Physically, these results could be an indication of heat transfer enhancement due to increasing surface area to volume ratio of the nanoparticles.

The model has also been run for CNT dimensions obtained from TEM images in Figure 2.16. Results for possible highest and lowest aspect ratio can be seen in Figure 4.12 and compared with the experimental data. These runs include the GA. with $\phi_{\mathrm{GA}} = 0.74$.

The extreme cases envelope the experimental data. While the experimental data are closer to lowest aspect ratio line, they are far from the highest aspect ratio line. TEM images show that nanotube length and diameters widely range, therefore when an average is taken, model estimates closer results to experimental data as shown in Figure 4.13. Whether the estimation falls into the uncertainty range, however, depends on other parameters like GA concentration and thermal

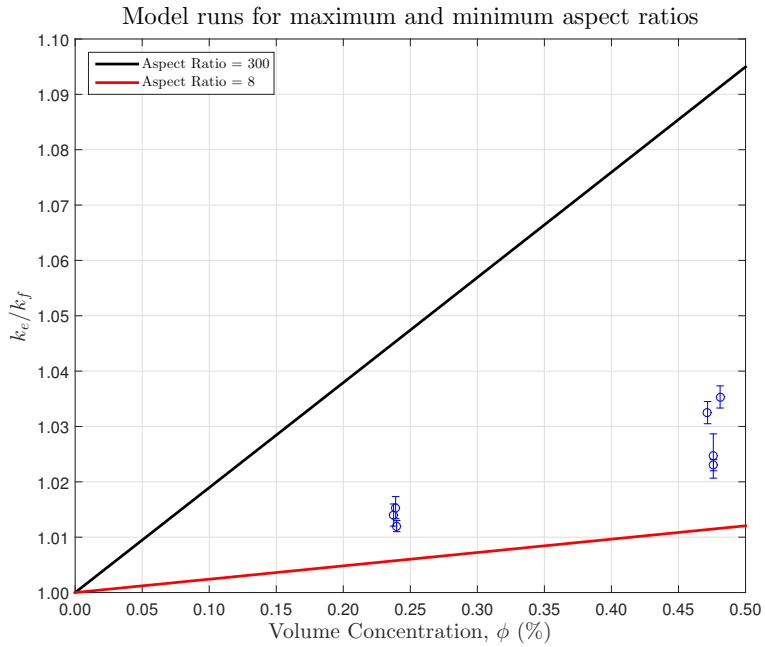

Figure 4.12: Model runs with lowest and highest AR compared with experimental data

conductivity as shown in Section 4.4.2 and Section 4.4.4.

4.4.6 Comparison of theoretical and experimental results

The MATLAB codes for RM and RHC models have been run to simulate the experimental conditions for comparison purposes. For each experimental data, (B1-B7) a corresponding run has been made with matching ϕ_{CNT} and ϕ_{GA} which in turn determined the value of the respective v. The thermal conductivity of GA has again been taken as 0.1 W/m·K and the empirical parameter κ for RHC has been taken as 1.55 for the reason explained in Section 4.4.3.

Results from the models are given in Figure 4.13. As expected, Renovated Hamilton Crosser models give closer results to the experimental data. However, while Renovated Maxwell model responds to the increase in GA as a less increase (or even a decrease) in overall thermal conductivity, which also physically makes sense, RHC model results in an irregular trend in thermal conductivity with increasing GA concentration, which has been discussed as the effect of layer

thickness in RHC in Section 4.4.2.

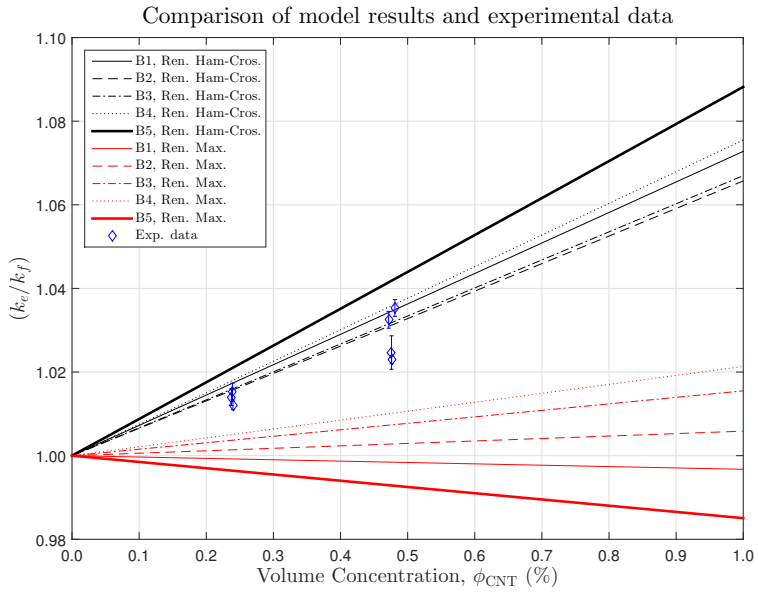

Figure 4.13: Comparison of experimental data and model runs

4.4.7 Comparison of RHC model with available experimental data in the literature

RHC model was run to compare its results with experimental data of Sadri *et al.* [30] and Indhuja *et al.* [31]. Models took the CNT and GA properties as given in the work of aforementioned authors. CNT lengths of Sadri *et al.* and Indhuja *et al.* were given as $10\,\mu m - 30\,\mu m$ and $5\,\mu m - 15\,\mu m$, respectively. Both work measure the thermal conductivity using KD2 Pro. Uncertainty values were only provided by Indhuja *et al.* Model runs are shown in Figure 4.14.

The model overpredicts the data of Indhuja *et al.* and underpredicts the data of Sadri *et al.* These results as well indicate the substantial effect of particle dimensions on thermal conductivity, since the only difference in the nanofluids of two work are the length of CNTs.

Overall, it has been found out that although a good agreement between the models and the 3ω measurements was shown, thermal conductivity estimations of the models are affected significantly by the changes in input parameters like

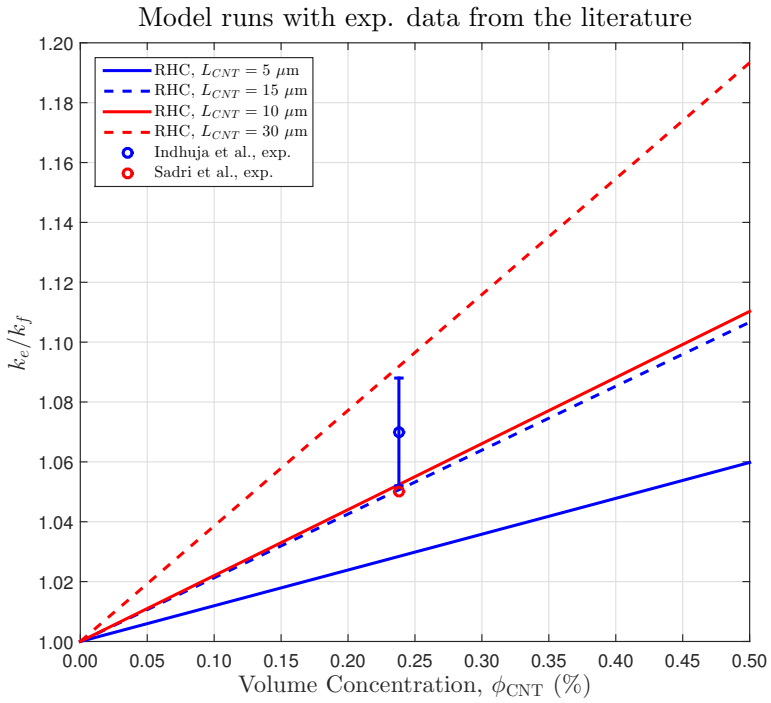

Figure 4.14: Model runs with experimental data from the literature

particle dimensions, layer thickness and layer conductivity and because it is difficult to precisely know the values of these parameters, this model can only be used to roughly estimate the thermal conductivity of nanofluids with surfactants.

4.5 Stability of the nanofluids

It could already be seen from Figure 2.18 that GA has the upmost importance when preparing a stable CNT nanofluid. More GA should have been used to fully disperse the CNT in water in the expense of thermal conductivity enhancement. On the other hand, a CNT-water mixture without surfactant precipitates in minutes and the mixture becomes colorless with all the CNT at bottom, contrary to samples prepared for this work.

Figure 4.15 shows the photographs of two samples, one from series A (4.15a) and one from series B (4.15b) taken about 10 months after their preparation.

Due to its lower concentration, sample from series A looks very stable, with no

(a) Sample from series A

(b) Sample from series B

Figure 4.15: Photos of CNT nanofluids with GA taken 10 months after preparation

adhesion of CNTs on the wall of the container. Trace amount of precipitate was present at the bottom of its container. The other sample is B5. Despite having the highest ϕ_{GA} to ϕ_{CNT} ratio among all the samples, CNTs still adhere on the surface of its container. However, there is still no color change in the sample after 10 months.

The thermal conductivities of samples B4 and B5, the samples with the lowest and highest GA to CNT concentration, were measured again 9 months after the first measurement. The results were the same as in the first measurement.

CHAPTER 5

CONCLUSION

5.1 Summary and conclusion

In this work, water based carbon nanotube nanofluids with GA as the surfactant have been prepared in different volumetric concentrations to investigate their thermal conductivities. A setup based on THW method was initially built for the measurements. It was found out that the built THW setup was not suitable for the samples to be measured and the experiments were continued using a different setup based on 3ω method. The results revealed an inverse proportionality between GA content and overall thermal conductivity. The results have also been compared with available data in the literature; thermal conductivity enhancement in the prepared samples has been found to be lower than most literature data. This is concluded to be caused by the differences in the steps in preparation of nanofluids.

The thermal conductivities of prepared nanofluids have also been investigated numerically by using two models, namely RM and RHC models, that were modified for use in this work. Experimental and numerical results have been found to be in good agreement.

A parametric study with the models has been carried out as well. The effects of particle dimensions, surfactant layer thickness and its thermal conductivity, the and empirical parameter, κ, in the RHC model have been investigated.

RHC model revealed that the particle dimensions greatly influence the overall

thermal conductivity of the nanofluid. It increases with increasing nanotube aspect ratio.

Both models have been shown to be very sensitive to the changes in layer thermal conductivity when it is significantly lower than that of the particle. It should be noted that the RM and RHC models consider a nanolayer having higher thermal conductivity than that of the base fluid. Hence, RM and RHC models as surfactant effect modelers should only be used to make a rough estimation of thermal conductivity.

5.2 Future work

As future work, there are a couple of things that can be done. Transient hot wire setup can be improved by developing a system to control the tightness of the wire. The middle section of the cell can be made of a transparent material in order to check the wire straightness visually. A longer wire can also be used for more reliable results.

The temperature dependence of thermal conductivity can be investigated by conducting the experiments in a temperature controlled environment. It is important to know the temperature effects on conductivity since heat transfer fluids operate on diverse temperature ranges.

Nanofluids with nanotubes of different dimensions can be prepared to analyze the effect of particle aspect ratio on overall thermal conductivity. The results may be compared with the corresponding ones from the models.

The viscosity of the CNT nanofluids have not been investigated thoroughly, although it is an important parameter for any practical use. Viscosities at different temperatures can be measured, and a performance analysis investigating the heat transfer enhancement vs. pumping power requirement can be conducted.

As for the numerical investigation, RM and RHC models are two of the earliest nanofluid thermal conductivity models. The investigation may be repeated with newer models for future comparison.

REFERENCES

[1] J. C. Maxwell. *A treatise on electricity and magnetism*. Clarendon Press, 2nd edition, 1873.

[2] S.U.S. Choi and J.A. Eastman. *Enhancing thermal conductivity of fluids with nanoparticles*. 1995.

[3] R. Saidur, K. Leong, and H. A. Mohammad. A review on applications and challenges of nanofluids. *Renewable and Sustainable Energy Reviews*, 15:1646–1668, 2011.

[4] C. T. Nguyen, G. R., C. Gauthier, and N. Galanis. Heat transfer enhancement using Al_2O_3–water nanofluid for an electronic liquid cooling system. *Applied Thermal Engineering*, 27(8–9):1501 – 1506, 2007.

[5] W. Jiang, G. Ding, and H. Peng. Measurement and model on thermal conductivities of CNT nanorefrigerants. *International Journal of Thermal Sciences*, 48:1108–1115, 2008.

[6] R. R. Srikant, D. N. Rao, M. S. Subrahmanyam, and V. P. Krishna. Applicability of cutting fluids with nanoparticle inclusion as coolants in machining. *Proceedings of the Institution of Mechanical Engineers, Part J: Journal of Engineering Tribology*, 223(2):221–225, 2009.

[7] L. Zhang, Y. Ding, M. Povey, and D. York. ZnO nanofluids – a potential antibacterial agent. *Progress in Natural Science*, 18(8):939 – 944, 2008.

[8] P. Keblinski, S. R. Phillpot, S. U. S. Choi, and J. A. Eastman. Mechanisms of heat flow in suspensions of nano-sized particles(nanofluids). *International Journal of Heat and Mass Transfer*, 45:855–863, 2002.

[9] S. P. Jang and S. U. S. Choi. Role of brownian motion in the enhanced thermal conductivity of nanofluids. *Applied Physics Letters*, 84(21):4316–4318, 2001.

[10] C. J. Yu, A. G. Richter, A. Datta, M. K. Durbin, and P. Dutta. Molecular layering in a liquid on a solid substrate: an X-ray reflectivity study. *Physica B*, 283:27–31, 2000.

[11] W. Williams, J. Buongiorno, and L. W. Hu. Experimental investigation of turbulent convective heat transfer and pressure loss of alumina/water

and zirconia/water nanoparticle colloids (nanofluids) in horizontal tubes. *ASME Journal of Heat Transfer*, 130, 2008.

[12] E. B. Elçioğlu, E. Şimşek, and T. Okutucu-Özyurt. Stability of nanofluids: Fundamentals, state-of-the-art, and potential applications. In *Microscale and Nanoscale Heat Transfer*, chapter 6, pages 155–181. CRC Press, 2016.

[13] E. Şimşek, E. B. Elçioğlu, and T. Okutucu-Özyurt. Stability of nanofluids-a critical review. In *Proceedings of CONV-14: International Symposium on Convective Heat and Mass Transfer. June 8 - 13, 2014, Kusadasi, Turkey*, 2014.

[14] M. F. L. De Volder, S. H. Tawfick, R. H. Baughman, and A. J. Hart. Carbon nanotubes: Present and future commercial applications. *Science*, 339(6119):535–539, 2013.

[15] S. S. Gupta, V. M. Siva, S. Krishnan, T. S. Sreeprasad, P. K. Singh, T. Pradeep, and S. K. Das. Thermal conductivity enhancement of nanofluids containing graphene nanosheets. *Journal of Applied Physics*, 110(8), 2011.

[16] S. Berber, Y. K. Kwon, and D. Tomanek. Unusually high thermal conductivity of carbon nanotubes. *Physical Review Letters*, 84(20):4613–4616, 2000.

[17] D. K. Devendiran and V. A. Amirtham. A review on preparation, characterization, properties and applications of nanofluids. *Renewable and Sustainable Energy Reviews*, 60:21–40, 2016.

[18] B. H. Thang, P. H. Khoi, and P. N. Minh. A modified model for the thermal conductivity of carbon nanotube nanofluids. *Physics of Fluids*, 27(3), 2015.

[19] P. Kim, L. Shi, A. Majumdar, and P. L. McEuen. Thermal transport measurements of individual multiwalled nanotubes. *Physical Review Letters*, 87, 2001.

[20] H. Xie and L. Chen. Review on the preparation and thermal performances of carbon nanotube contained nanofluids. *Journal of Chemical & Engineering Data*, 16:1030–1041, 2011.

[21] S. U. S. Choi, Z. G. Zhang, W. Yu, F. E. Lockwood, and E. A. Grulke. Anomalous thermal conductivity enhancement in nanotube suspensions. *Applied Physics Letters*, 79(14):2252–2254, 2001.

[22] H. Xie, H. Lee, W. Youn, and M. Choi. Nanofluids containing multiwalled carbon nanotubes and their enhanced thermal conductivities. *Journal of Applied Physics*, 94(8):4967–4971, 2003.

[23] H. Xie and L. Chen. Adjustable thermal conductivity in carbon nanotube nanofluids. *Physics Letters A*, 373:1861–1864, 2009.

[24] M. J. Assael, C. F. Chen, I. Metaxa, and W. A. Wakeham. Thermal conductivity of suspensions of carbon nanotubes in water. *International Journal of Thermophysics*, 25(4):971–985, 2004.

[25] D. Wen and Y. Ding. Effective thermal conductivity of aqueous suspensions of carbon nanotubes (carbon nanotube nanofluids). *Journal of Thermophysics and Heat Transfer*, 18(4):481–485, 2004.

[26] Y. Ding, H. Alias, D. Wen, and R. A. Williams. Heat transfer of aqueous suspensions of carbon nanotubes (CNT nanofluids). *International Journal of Heat and Mass Transfer*, 49:240–250, 2006.

[27] S. Halelfadl, T. Mare, and P. Estelle. Efficiency of carbon nanotubes water based nanofluids as coolants. *Experimental Thermal and Fluid Science*, 53:104–110, 2013.

[28] Y. J. Hwang, Y. C. Ahn, H. S. Shin, C. G Lee, G. T. Kim, H. S. Park, and J. K. Lee. Investigations on characteristics of thermal conductivity enhancement of nanofluids. *Current Applied Physics*, 6:1068–1071, 2006.

[29] W. Rashmi, A. F. Ismail, I. Sopyan, A. T. Jameel, F. Yusof, M. Khalid, and M. N. Mubarak. Stability and thermal conductivity enhancement of carbon nanotube nanofluid using gum arabic. *Journal of Experimental Nanoscience*, 6(6):567–579, 2011.

[30] R. Sadri, G. Ahmadi, H. Togun, M. Dahari, S. N. Kazi, E. Sadeghinezad, and N. Zubir. An experimental study on thermal conductivity and viscosity of nanofluids containing carbon nanotubes. *Nanoscale Research Letters*, 9(1):1–16, 2014.

[31] A Indhuja, K. S. Suganthi, S. Manikandan, and K. S. Rajan. Viscosity and thermal conductivity of dispersions of gum arabic capped mwcnt in water: Influence of MWCNT concentration and temperature. *Journal of the Taiwan Institute of Chemical Engineers*, 44:474–479, 2013.

[32] A. Nasiri, M. Shariaty-Niasar, A. M. Rashidi, and R. Khodafarin. Effect of CNT structures on thermal conductivity and stability of nanofluid. *International Journal of Heat and Mass Transfer*, 55:1529–1535, 2012.

[33] H. M. Roder. A transient hot wire thermal conductivity apparatus for fluids. *Journal of Research of National Bureau of Standards*, 86(5), 1981.

[34] G. Paul, M. Chopkar, I. Manna, and P. K. Das. Techniques for measuring the thermal conductivity of nanofluids: A review. *Renewable and Sustainable Energy Reviews*, 14:1913–1924, 2010.

[35] H. S. Carslaw and J. C. Jaeger. *Conduction of heat in solids.* Oxford University Press, 2nd edition, 1959.

[36] W. T. Kierkus, N. Mani, and J. E. S. Venart. Radial-axial transient heat conduction in a region bounded internally by a circular cylinder of finite length and appreciable heat capacity. *Canadian Journal of Physics*, 51(11):1182–1186, 1973.

[37] Y. Nagasaka and A. Nagashima. Absolute measurement of thermal conductivity of electrically conducting liquids by the transient hot-wire method. *Journal of Physics E: Scientific Instruments*, 14:1435–1440, 1981.

[38] M. Kostic and K. C. Simham. Computerized, transient hot-wire thermal conductivity (hwtc) apparatus for nanofluids. In *Proceedings of the 6th WSEAS International Conference on Heat and Mass Transfer*, 2009.

[39] S. Lee, S. U. S. Choi, S. Li, and J. A. Eastman. Measuring thermal conductivity of fluids containing oxide nanoparticles. *Journal of Heat Transfer*, 121:280–289, 1999.

[40] D. de Koninck. Thermal conductivity measurements using the 3-omega technique: Application to power harvesting microsystems. Master's thesis, McGill University, 2008.

[41] D.-W. Oh, A. Jain, J. K. Eaton, K. E. Goodson, and J. S. Lee. Thermal conductivity measurement and sedimentation detection of aluminum oxide nanofluids by using the 3ω method. *International Journal of Heat and Fluid Flow*, 29(5):1456–1461, 2008.

[42] A. Turgut, I. Tavman, M. Chirtoc, H. P. Schuchmann, C. Sauter, and S. Tavman. Thermal conductivity and viscosity measurements of water-based tio2 nanofluids. *International Journal of Thermophysics*, 30(4):1213–1226, 2009.

[43] G. S. Wu, J. K. Yang, S. L. Ge, Y. J. Wang, M. H. Chen, and Y. F. Chen. Thermal conductivity measurement for carbon-nanotube suspensions with 3ω method. In *Advanced Materials Research*, volume 60, pages 394–398. Trans Tech Publ, 2009.

[44] Tae Y Choi, Mohammad H Maneshian, Boseon Kang, Won S Chang, Chang S Han, and Dimos Poulikakos. Measurement of the thermal conductivity of a water-based single-wall carbon nanotube colloidal suspension with a modified $3-\omega$ method. *Nanotechnology*, 20(31):315706, 2009.

[45] J.-F. Hoffmann, J.-F. Henry, G. Vaitilingom, R. Olives, M. Chirtoc, D. Caron, and X. Py. Temperature dependence of thermal conductivity of vegetable oils for use in concentrated solar power plants, measured

by 3omega hot wire method. *International Journal of Thermal Sciences*, 107:105 – 110, 2016.

[46] A. Turgut, C. Sauter, M. Chirtoc, F. J. Henry, S. Tavman, I. Tavman, and J. Pelzl. Ac hot wire measurement of thermophysical properties of nanofluids with 3ω method. *The European Physical Journal Special Topics*, 153(1):349–352, 2008.

[47] R. L. Hamilton and O. K. Crosser. Thermal conductivity of heterogeneous two-component systems. *Industrial & Engineering Chemistry Fundamentals*, 1(3):187–191, 1962.

[48] W. Yu and S. U. S. Choi. The role of interfacial layers in the enhanced thermal conductivity of nanofluids: A renovated Maxwell model. *Journal of Nanoparticle Research*, 5:167–171, 2003.

[49] W. Yu and S. U. S. Choi. The role of interfacial layers in the enhanced thermal conductivity of nanofluids: A renovated Hamilton-Crosser model. *Journal of Nanoparticle Research*, 6:355–361, 2004.

[50] B. X. Wang, L. P. Zhou, and X. F. Peng. A fractal model for predicting the effective thermal conductivity of liquid with suspension of nanoparticles. *International Journal of Heat and Mass Transfer*, 46:2665–2762, 2003.

[51] C. W. Nan, Z. Shi, and Y. Lin. A simple model for thermal conductivity of carbon nanotube-based composites. *Chemical Physics Letters*, 375:666–669, 2003.

[52] C. W. Nan, G. Liu, Y. Lin, and M. Li. Interface effect on thermal conductivity of carbon nanotube composites. *Applied Physics Letters*, 85(16):3549–3551, 2004.

[53] P. Bhattacharya, S. K. Saha, A. Yadav, P. H. Phelan, and R. S. Prasher. Brownian dynamics simulation to determine the effective thermal conductivity of nanofluids. *Journal of Applied Physics*, 95(11):6492–6494, 2004.

[54] K. C. Leong, C. Yang, and S. M. S. Murshed. A model for the thermal conductivity of nanofluids – the effect of interfacial layer. *Journal of Nanoparticle Research*, 8:245–254, 2006.

[55] K. C. Leong, C. Yang, and S. M. S. Murshed. A combined model for the thermal conductivity of nanofluids. *Applied Thermal Engineering*, 29:2477–2483, 2009.

[56] H. Xie, M. Fujii, and X. Zhang. Effect of interfacial nanolayer on the effective thermal conductivity of nanoparticle-fluid mixture. *International Journal of Heat and Mass Transfer*, 48:2926–2932, 2005.

[57] P. Tillman and J. M. Hill. A new model forthermal conductivity of nanofluids. In *Proceedings of 2006 International Conference On Nanoscience and Nanotechnology*, 2006.

[58] P. Tillman and J. M. Hill. Determination of nanolayer thickness for a nanofluid. *International Communications in Heat and Mass Transfer*, 34(4):399–407, 2007.

[59] H. E. Patel, K. B. Anoop, T. Sundararajan, and S. K. Das. Model for thermal conductivity of CNT nanofluids. *Bulletin of Material Science*, 31(3):387–390, 2008.

[60] B. H. Thang, P. H. Khoi, and P. N. Minh. A modified model for thermal conductivity of carbon nanotube-nanofluids. *Physics of Fluids*, 27, 2015.

[61] Y. Feng, B. Yu, and M. Zou. The effective thermal conductivity of nanofluids based on the nanolayer and the aggregation of nanoparticles. *Journal of Physics D: Applied Physics*, 40:3164–3171, 2007.

[62] L. Yang and K. Du. A thermal conductivity model for low concentrated nanofluids containing surfactants under various dispersion types. *International Journal of Refrigeration*, 35:1978–1988, 2012.

[63] W. Yu and S. U.-S. Choi. Influence of insulation coating on thermal conductivity measurement by transient hot-wire method. *Review of Scientific Instruments*, 77(7), 2006.

[64] D. G. Cahill. Thermal conductivity measurement from 30 to 750 k: the 3ω method. *Review of Scientific Instruments*, 61(2):802–808, 1990.

[65] Humancorp > water purification system > zeneer power (toc):. `http://humancorp.co.kr/g4/bbs/board.php?bo_table=eng_001&wr_id=23`. Accessed: 2016-05-16.

[66] MWCNTs ()95% , OD (7nm). `http://www.us-nano.com/inc/sdetail/215`. Accessed: 2016-05-11.

[67] 104228 | Gum arabic. `http://www.merckmillipore.com/TR/tr/product/Gum-arabic,MDA_CHEM-104228`. Accessed: 2016-05-11.

[68] M. C. Llaguno, J. Hone, A. T. Johnson, and J. E. Fischer. Thermal conductivity of single wall carbon nanotubes: diameter and annealing dependence. *arXiv preprint cond-mat/0108142*, 2001.

APPENDIX A

TECHNICAL DRAWINGS

Technical drawings of the hot wire cell used in THW setup are given in figures A.1, A.2 and A.3. All dimensions are in mm.

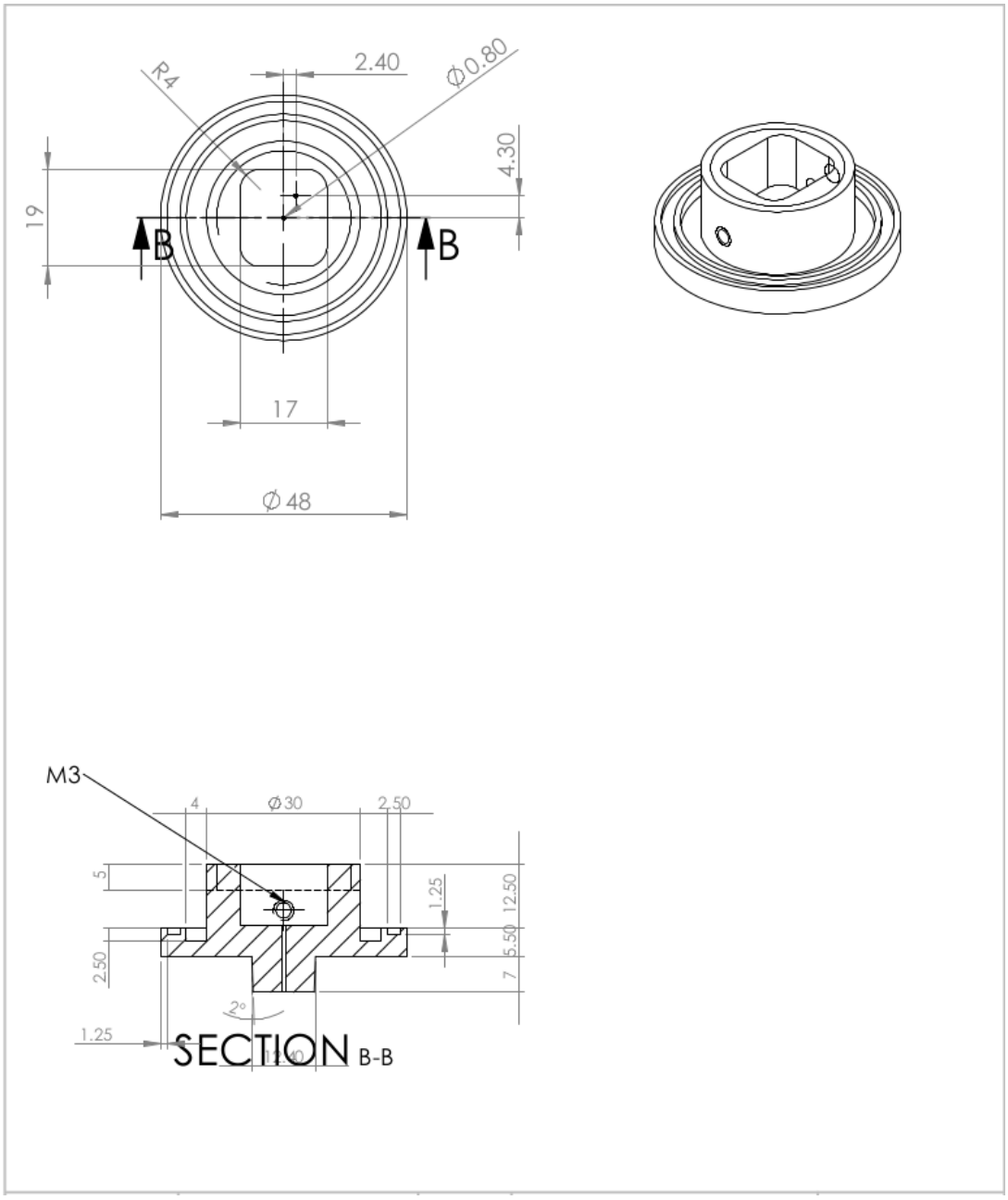

Figure A.1: Wire holder of the hot wire cell

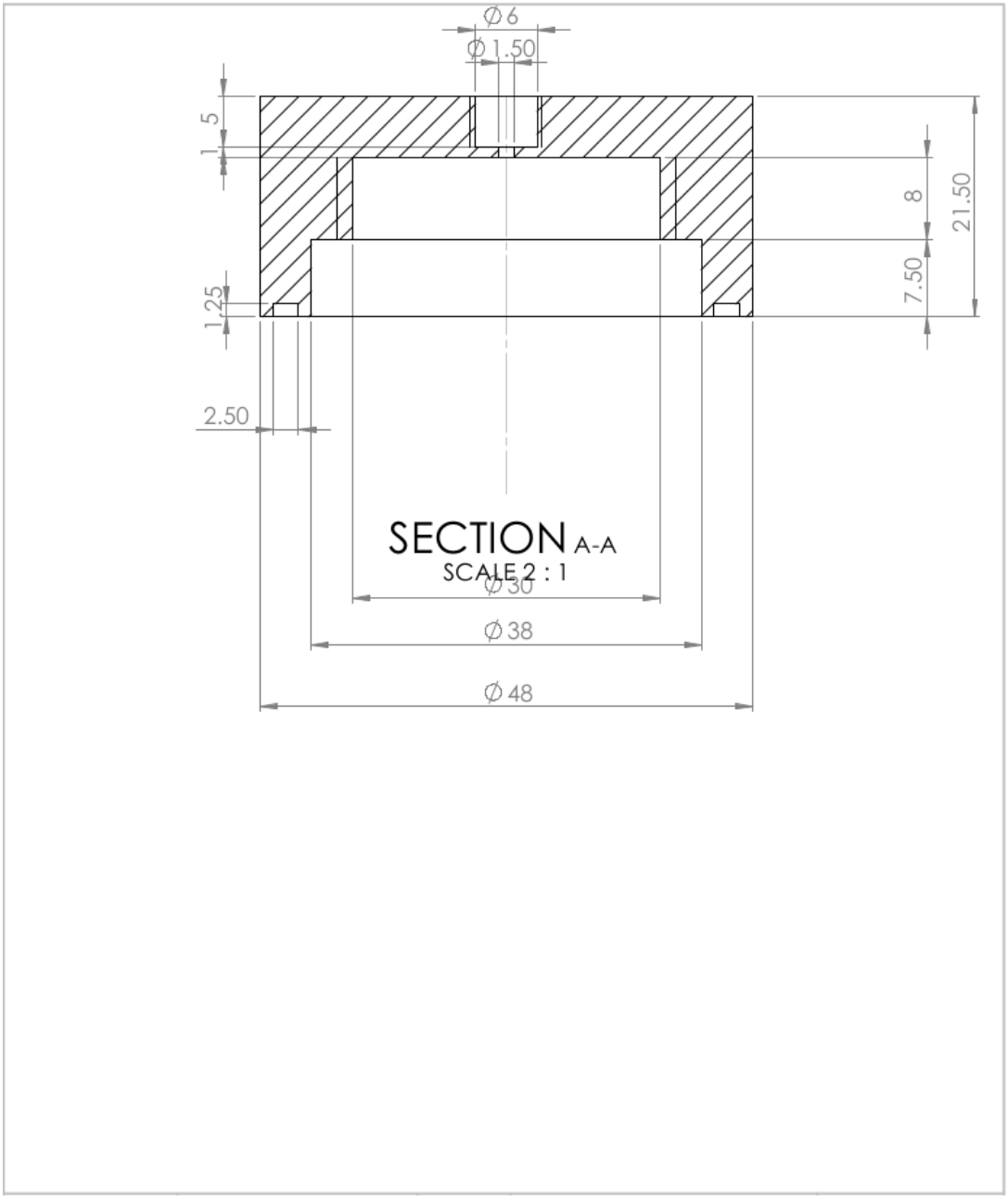

Figure A.2: Lid of the holder

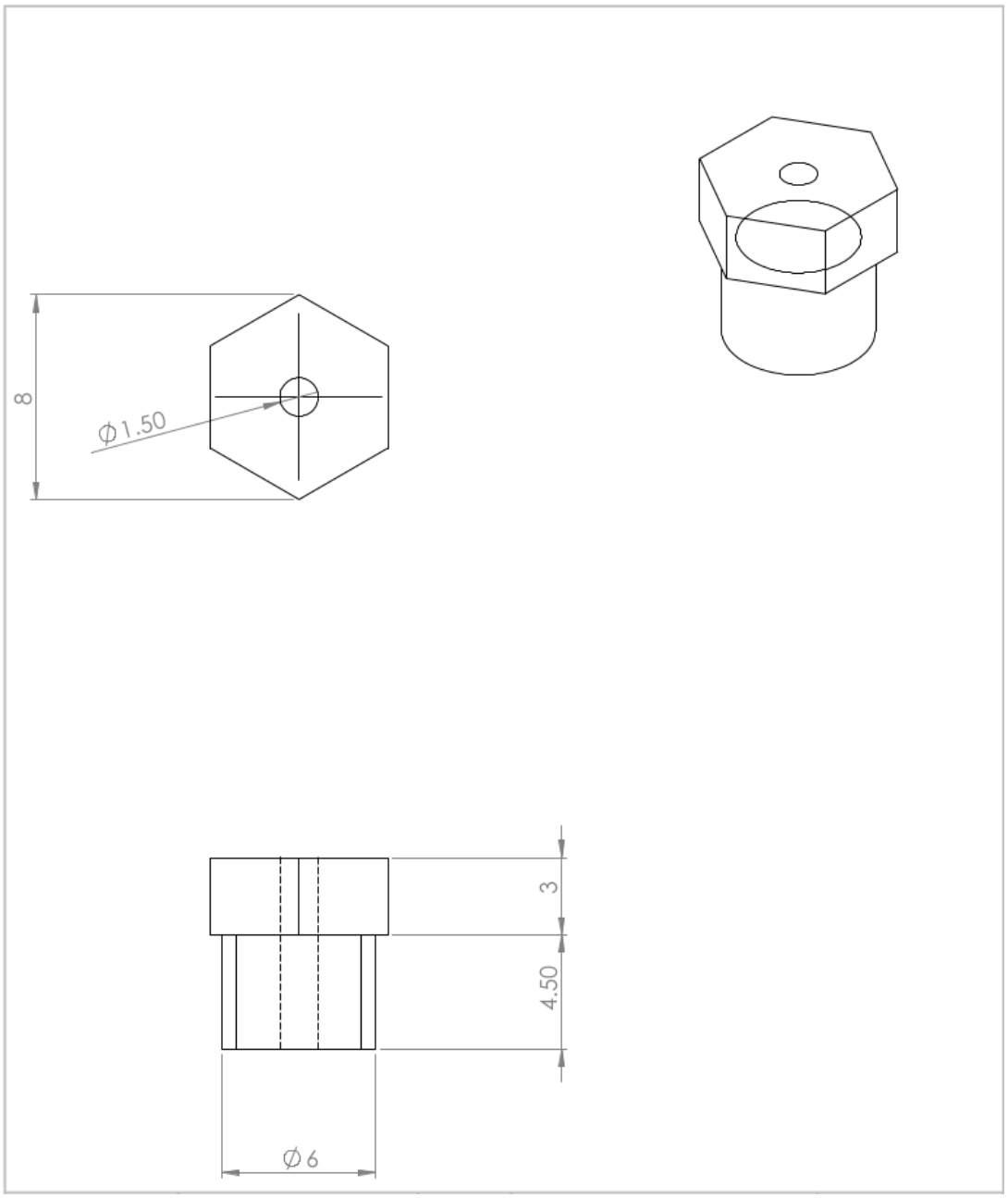

Figure A.3: Leakage prevention element

APPENDIX B

PREPARED NANOFLUID SPECIFICATIONS

Table B.1: Composition and uncertainty in ϕ of prepared nanofluids

Sample Name	CNT (mg)	Water (g)	GA (mg)	$u_{\phi_{\mathrm{CNT}}}$ (%)	$u_{\phi_{\mathrm{GA}}}$ (%)
A1	40.1	79.9624	10.5	5.01	5.08
A2	40.4	79.9605	10.0	5.01	5.09
A3	20.2	79.9806	5.2	5.02	5.29
A4	10.1	79.992	2.5	5.12	6.66
A5	40	79.9601	9.9	5.00	5.02
A6	40.2	79.9605	10.1	5.01	5.10
A7	40.2	79.9613	10.3	5.01	5.09
A8	40	79.96	10.1	5.01	5.10
B2	300.6	29.97	75.4	5.00	5.00
B1	299.8	29.5421	151.6	5.00	5.00
B3	303.2	29.68	31.2	5.00	5.01
B4	300	29.6875	15.2	5.00	5.04
B5	149.6	29.695	149.7	5.00	5.00
B6	150.6	29.7746	75.6	5.00	5.00
B7	151.1	29.8183	38.1	5.00	5.01